

Surface Bogoliubov-Dirac cones and helical Majorana hinge modes in superconducting Dirac semimetals

Majid Kheirkhah,¹ Zheng-Yang Zhuang,² Joseph Maciejko,^{1,3} and Zhongbo Yan^{2,*}

¹*Department of Physics, University of Alberta, Edmonton, Alberta T6G 2E1, Canada*

²*School of Physics, Sun Yat-Sen University, Guangzhou 510275, China*

³*Theoretical Physics Institute, University of Alberta, Edmonton, Alberta T6G 2E1, Canada*

(Dated: January 17, 2022)

In the presence of certain symmetries, three-dimensional Dirac semimetals can harbor not only surface Fermi arcs, but also surface Dirac cones. Motivated by the experimental observation of rotation-symmetry-protected Dirac semimetal states in iron-based superconductors, we investigate the potential intrinsic topological phases in a C_{4z} -rotational invariant superconducting Dirac semimetal with s_{\pm} -wave pairing. When the normal state harbors only surface Fermi arcs on the side surfaces, we find that an interesting gapped superconducting state with a quartet of Bogoliubov-Dirac cones on each side surface can be realized, even though the first-order topology of its bulk is trivial. When the normal state simultaneously harbors surface Fermi arcs and surface Dirac cones, we find that a second-order time-reversal invariant topological superconductor with helical Majorana hinge states can be realized. The criteria for these two distinct topological phases have a simple geometric interpretation in terms of three characteristic surfaces in momentum space. By reducing the bulk material to a thin film normal to the axis of rotation symmetry, we further find that a two-dimensional first-order time-reversal invariant topological superconductor can be realized if the inversion symmetry is broken by applying a gate voltage. Our work reveals that diverse topological superconducting phases and types of Majorana modes can be realized in superconducting Dirac semimetals.

I. INTRODUCTION

Topological superconductors (TSCs) are a class of novel phases with exotic gapless boundary excitations known as Majorana modes^{1,2}. Over the past decade, the pursuit of TSCs and Majorana modes in real materials has attracted a great amount of enthusiasm^{3–11}, owing to their exotic properties and potential applications in topological quantum computation^{12–15}. Very recently, an important form of progress on the theoretical side is the birth of the concept named higher-order TSCs^{16–27}, which not only enriches the physics of TSCs, but also provides new perspectives for the realization and applications of Majorana modes^{28–66}. The most prominent difference between conventional TSCs and their higher-order counterparts lies in the bulk-boundary correspondence, or more precisely, the codimension d_c of the gapless Majorana modes at the boundary. To be specific, a conventional TSC has $d_c = 1$, while an n th-order TSC has $d_c = n \geq 2$. Conventional TSCs are thus also dubbed as first-order TSCs. One direct significance of this extension is that a lot of systems previously thought to be trivial in the framework of first-order topology are recognized to be nontrivial in the framework of higher-order topology.

Because of the scarcity of odd-parity superconductors in nature, the realization of both first-order and second-order TSCs heavily relies on materials with strong spin-orbit coupling or topological band structure^{24,25,35,43,67–71}. By far, most experiments in this field have focused on the realization of first-order TSCs in various kinds of heterostructures which simultaneously consist of three ingredients, namely, spin-orbit

coupling, magnetism or external magnetic fields, and s -wave superconductivity^{72–81}. Despite steady progress in experiments, the complexity of such heterostructures and the concomitant strong inhomogeneity make a definitive confirmation of the expected Majorana modes remain elusive^{82–84}. Since these common shortcomings of heterostructures shadow the pursuit of Majorana modes and are quite challenging to overcome in the short term, intrinsic TSCs become highly desired to make further breakthroughs. Remarkably, the band structures of a series of iron-based superconductors have recently been observed to host both topological insulator states and rotation-symmetry-protected Dirac semimetal (DSM) states near the Fermi level^{85,86}. Since the coexistence of topological insulator states and superconductivity provides a realization of the Fu-Kane proposal⁶⁷ in a single material, the potential existence of Majorana zero modes in the vortices of these iron-based superconductors has attracted great attention^{87–97}. In addition, it turns out that the combination of topological insulator states and unconventional s_{\pm} -wave pairing also makes these iron-based superconductors promising for the realization of intrinsic higher-order TSCs^{32,97}. Compared with the topological insulator states, we notice that the DSM states in these iron-based superconductors have been explored much less^{98–101}.

Motivated by the above observation, we explore the potential intrinsic topological phases in superconducting DSMs with s_{\pm} -wave pairing. However, instead of considering a realistic but complicated Hamiltonian to accurately produce the band structure of one specific iron-based superconductor, we will take a minimal-Hamiltonian approach for generality, so that the results

can be applied to all DSMs with the same symmetry and topological properties. To be relevant to iron-based superconductors, in this paper we focus on DSMs protected by C_{4z} -rotation symmetry¹⁰². For DSMs, while the low-energy physics in the bulk can be universally described by linear continuum Dirac Hamiltonians, the gapless states on the boundary, however, are sensitive to the details of the full lattice Hamiltonian. An important fact is that both surface Fermi arcs and surface Dirac cones are symmetry allowed in DSMs^{100,103–105}. As a consequence, we find that depending on whether surface Fermi arcs and surface Dirac cones coexist or not, a second-order time-reversal invariant TSC with helical Majorana hinge modes or an interesting gapped phase with a quartet of Bogoliubov-Dirac cones on each side surface can be realized in the superconducting DSM, respectively. By reducing the dimension of the second-order time-reversal invariant TSC from three dimensions to a thin film, we find that a first-order time-reversal invariant TSC can be realized if the inversion symmetry is broken by applying an external gate voltage. These findings suggest that the superconducting DSM on its own can realize a diversity of intrinsic TSCs.

The paper is organized as follows. In Sec. II, the topological properties of the normal state are investigated. In Sec. III, we show that two superconducting phases with distinct topological boundary states can be realized in superconducting DSMs. In Sec. IV, we show that thin films of a superconducting DSM can realize first-order time-reversal invariant TSCs. Finally, we conclude with a discussion in Sec. V. Some calculation details are relegated to Appendices A and B.

II. TOPOLOGICAL PROPERTIES OF THE NORMAL STATE

We start with the DSM Hamiltonian which, in the basis $\psi_{\mathbf{k}}^\dagger = (c_{a,\uparrow,\mathbf{k}}^\dagger, c_{b,\uparrow,\mathbf{k}}^\dagger, c_{a,\downarrow,\mathbf{k}}^\dagger, c_{b,\downarrow,\mathbf{k}}^\dagger)$, reads¹⁰²

$$H_{\text{DSM}}(\mathbf{k}) = [m - t(\cos k_x + \cos k_y) - t_z \cos k_z] \sigma_z + \lambda \sin k_x s_z \sigma_x + \eta \sin k_z (\cos k_x - \cos k_y) s_x \sigma_x - \lambda \sin k_y \sigma_y + 2\eta \sin k_x \sin k_y \sin k_z s_y \sigma_x, \quad (1)$$

where the Pauli matrices σ_i and s_i act on the orbital (a, b) and spin (\uparrow, \downarrow) degrees of freedom, respectively. For notational simplicity, the lattice constants are set to unity throughout this paper, and identity matrices are always made implicit. The Hamiltonian simultaneously has time-reversal symmetry ($\mathcal{T} = is_y \mathcal{K}$, with \mathcal{K} denoting complex conjugation), inversion symmetry ($I = \sigma_z$), and C_{4z} -rotation symmetry ($C_{4z} = \text{diag}\{e^{-3i\pi/4}, e^{-i\pi/4}, e^{3i\pi/4}, e^{i\pi/4}\}$), which thus allows the presence of robust Dirac points on the rotation symmetry axis. It is easy to find that Dirac points will appear as long as the band inversion surface (BIS), which is defined as the zero-value contour of $m - t(\cos k_x + \cos k_y) - t_z \cos k_z$ in momentum space, encloses one time-reversal invariant momentum.

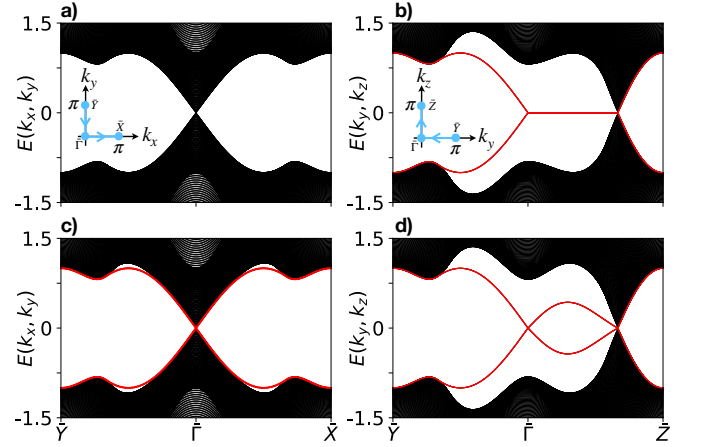


FIG. 1. (Color online) Surface band structure for the normal state. Common parameters are $m = 3$, $t = t_z = 2$, $\lambda = 1$. $\eta = 0$ in (a) and (b), and $\eta = 0.5$ in (c) and (d). Surface Dirac cones are absent in (a) and (b) and present in (c) and (d) at the center of the surface Brillouin zone. In each panel, the side with open boundary conditions is 200 lattice sites long.

Usually, as the two symmetry-allowed η terms in Eq. (1) only contribute cubic-order terms in momentum to the continuum Dirac Hamiltonian, they are neglected. While it is true that their higher-order contributions to the bulk can be safely neglected when focusing on the low-energy physics near the Dirac points, it has been demonstrated that their impact on the surface states, however, is significant^{100,104,106}. Without the two η terms ($\eta = 0$), the DSM is found to harbor only Fermi arcs on the side surfaces. Remarkably, once the two η terms are present ($\eta \neq 0$), the DSM harbors not only Fermi arcs on the side surfaces, but also a single Dirac cone on each of the surfaces of a cubic-geometry sample, resembling the surface Dirac cones in strong topological insulators. To have an intuitive picture of the qualitative difference between $\eta = 0$ and $\eta \neq 0$, we take $\{m, t, t_z, \lambda\} = \{3, 2, 2, 1\}$ so that the Dirac points are localized at $\mathbf{k}_{D,\pm} = \pm(0, 0, 2\pi/3)$ and then diagonalize the Hamiltonian in a cubic geometry with open boundary conditions in one direction and periodic boundary conditions in the other two orthogonal directions. The corresponding energy spectra shown in Fig. 1 clearly manifest the qualitative difference in surface states between $\eta = 0$ and $\eta \neq 0$. As we will show below, this remarkable difference will lead to distinct topological superconducting states.

III. TOPOLOGICAL PROPERTIES OF SUPERCONDUCTING DIRAC SEMIMETALS

Let us now focus on the superconducting state. Within the mean-field framework, the Hamiltonian becomes $H = \frac{1}{2} \sum_{\mathbf{k}} \Psi_{\mathbf{k}}^\dagger H_{\text{BdG}}(\mathbf{k}) \Psi_{\mathbf{k}}$, with $\Psi_{\mathbf{k}}^\dagger = (\psi_{\mathbf{k}}^\dagger, \psi_{-\mathbf{k}})$ and the corresponding Bogoliubov-de Gennes (BdG) Hamiltonian

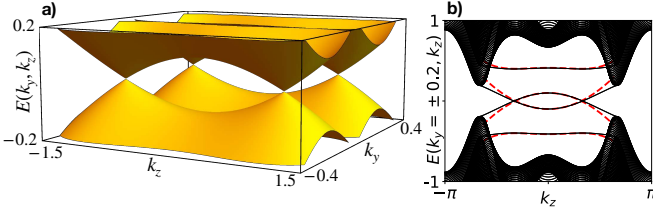


FIG. 2. (Color online) Chosen parameters are $m = 3$, $t = t_z = 2$, $\lambda = 1$, $\eta = 0$, $\mu = 0.2$, and $\Delta_0 = \Delta_s = 0.2$. Accordingly, $R_{\text{FS}} = 0.2$, $R_{\text{PNS}} = \sqrt{2}$, and $R_{\text{BIS}} = \sqrt{3}$. (a) The two middle bands of the surface Hamiltonian in Eq. (4) touch at $(k_y, k_z) = (\pm 0.2, \pm 1)$, forming four gapless Bogoliubov-Dirac cones. (b) Energy spectrum along $k_y = \pm 0.2$. The surface bands obtained from the low-energy analytical approach (midgap red dashed lines) agree excellently with those obtained by directly diagonalizing the full lattice Hamiltonian (midgap black solid lines, doubly degenerate) under open boundary conditions in the x direction, confirming the existence of four gapless Bogoliubov-Dirac cones on each of the two x -normal surfaces.

takes the form

$$H_{\text{BdG}}(\mathbf{k}) = \begin{pmatrix} H_{\text{DSM}}(\mathbf{k}) - \mu & -is_y \Delta(\mathbf{k}) \\ is_y \Delta(\mathbf{k}) & \mu - H_{\text{DSM}}^*(-\mathbf{k}) \end{pmatrix}, \quad (2)$$

where $\Delta(\mathbf{k}) = \Delta_0 - \Delta_s(\cos k_x + \cos k_y)$ characterizes the s_{\pm} -wave pairing. Since the BdG Hamiltonian simultaneously has time-reversal symmetry and particle-hole symmetry, it belongs to the DIII class in the ten-fold way classification^{107,108}. Accordingly, its first-order topology is characterized by a winding number N_w and follows a \mathbb{Z} classification in three dimensions. When N_w is a nonzero integer in a gapped superconductor, the bulk-boundary correspondence tells us that there are N_w robust Majorana cones on an arbitrary surface^{109–111}, irrespective of its orientation. A simple formula for N_w valid in the weak-pairing limit is¹¹²

$$N_w = \frac{1}{2} \sum_n \text{sgn}(\Delta_i) C_{1i}, \quad (3)$$

where C_{1i} denotes the first Chern number and $\text{sgn}(\Delta_i)$ denotes the sign of pairing on the i th Fermi surface. Since the simultaneous preservation of time-reversal symmetry and inversion symmetry forces C_{1i} to vanish, N_w thus identically vanishes, indicating that the first-order topology is always trivial for this Hamiltonian. Despite the absence of nontrivial first-order topology, the superconducting DSM, nevertheless, can be nontrivial in the higher-order topology and host interesting Majorana modes on the boundary.

The bulk spectrum of the superconducting DSM is gapped as long as the pairing node surface (PNS), which is the zero-value contour of $\Delta(\mathbf{k})$ in momentum space, does not cross the Fermi surface. On the boundary, the presence of superconductivity is also expected to gap out the topological surface states. An interesting question is whether it is possible that while the bulk states are

fully gapped, the topological surface states are not fully gapped, so that there emerge certain types of gapless Bogoliubov quasiparticles on the boundary. We find that the answer is affirmative. To show this, the most intuitive approach is to derive the low-energy Hamiltonian for the surface states. Without loss of generality, we focus on the left x -normal surface and assume that the parameters m , t , and t_z are chosen such that the BIS encloses the time-reversal invariant momentum $\Gamma = (0, 0, 0)$. Following a standard approach, we expand the lattice Hamiltonian around Γ to obtain the continuum bulk Hamiltonian and then find that the corresponding low-energy surface Hamiltonian takes the form (see Appendix A)

$$H_s(k_y, k_z) \approx \lambda k_y s_z + v_z(k_y, k_z) k_z \tau_z s_y - \mu \tau_z + \frac{\Delta_s}{2} \left(R_{\text{BIS}}^2 - R_{\text{PNS}}^2 - \frac{t_z}{t} k_z^2 \right) \tau_y s_y, \quad (4)$$

where $v_z(k_y, k_z) = -\eta(\tilde{m} + tk_y^2 + t_z k_z^2/2)/t$ with $\tilde{m} = m - 2t - t_z$, $R_{\text{BIS}} = \sqrt{-2\tilde{m}/t}$, and $R_{\text{PNS}} = \sqrt{-2\tilde{\Delta}/\Delta_s}$ with $\tilde{\Delta} = \Delta_0 - 2\Delta_s$. Here, we have already assumed $\{t, t_z, \lambda, \Delta_s\} > 0$ and $\{\tilde{m}, \tilde{\Delta}\} < 0$. According to the continuum bulk Hamiltonian, R_{BIS} and R_{PNS} correspond to the radii of BIS and PNS in the $k_z = 0$ plane, respectively. It is worth noting that the surface states only exist in the regime satisfying $tk_y^2 + t_z k_z^2 < -2\tilde{m}$, which is just the projection of BIS in the k_x direction.

Let us first consider the $\eta = 0$ case, where $v_z = 0$ in this limit. Accordingly, the normal state has only Fermi arcs which are two straight lines at $k_y = \pm R_{\text{FS}}$, where $R_{\text{FS}} = |\mu/\lambda|$ corresponds to the maximum radius of the Fermi surface in the k_x - k_y plane. The geometric meaning of this expression is that the Fermi arcs tangentially connect with the projection of the Fermi surface in the surface Brillouin zone¹¹³. Taking into account superconductivity, we find from Eq. (4) that the surface energy bands harbor four cones with linear dispersion at $(k_y, k_z) = (\pm R_{\text{FS}}, \pm \sqrt{t(R_{\text{BIS}}^2 - R_{\text{PNS}}^2)/t_z})$ if $R_{\text{BIS}} > R_{\text{PNS}}$. As the Bogoliubov quasiparticle operators associated with these surface cones do not satisfy the self-conjugate property ($\gamma_{\mathbf{k}}^\dagger = \gamma_{-\mathbf{k}}$ with $\gamma_{\mathbf{k}}^\dagger$ denoting the quasiparticle creation operator at momentum \mathbf{k}), we dub them Bogoliubov-Dirac cones to distinguish them from charge-neutral Majorana cones. Recalling that the precondition for this result is $tk_y^2 + t_z k_z^2 < -2\tilde{m}$, we find that the criterion for the existence of surface Bogoliubov-Dirac cones needs to be modified as $R_{\text{FS}} < R_{\text{PNS}} < R_{\text{BIS}}$. This criterion corresponds to a simple geometric picture, namely, the PNS simultaneously encloses the bulk Fermi surface and intersects the BIS. In Fig. 2, we provide numerical results to show the existence of four gapless Bogoliubov-Dirac cones on each of the side surfaces (note that the system has C_{4z} -rotation symmetry) when the above-mentioned criterion is fulfilled. Before proceeding to $\eta \neq 0$, it is worth pointing out that every gapless Bogoliubov-Dirac cone has a topological protection due to the existence of chiral symmetry (the product of particle-hole symmetry and time-reversal symmetry)

which will assign a topological winding number to characterize the band touching points of the surface energy spectrum¹¹⁴ (see Appendix A). Accordingly, one gapless Bogoliubov-Dirac cone can be gapped only when it meets another gapless Bogoliubov-Dirac cone characterized by an opposite winding number.

Now we turn to the $\eta \neq 0$ case for which surface Fermi arcs and Dirac cones coexist in the normal state. According to Eq. (4), we find that if the energy spectrum harbors gapless Bogoliubov-Dirac cones at $\eta = 0$, these persist for nonzero η as long as $|\eta| < \eta_c = \frac{2|\mu|}{R_{\text{PNS}}^2} \sqrt{t(R_{\text{BIS}}^2 - R_{\text{PNS}}^2)}$. However, with the increase in η , the surface Bogoliubov-Dirac cones approach one another and become gapped pairwise when $|\eta| > \eta_c$, resulting in a fully gapped surface energy spectrum (see Appendix A). Remarkably, after gapping out the surface Bogoliubov-Dirac cones, we find that the superconductor becomes a second-order time-reversal invariant TSC with helical Majorana hinge modes. To have an intuitive understanding of this transition, here we take the special case with $\mu = 0$ for an analytical illustration. For this special case, $\eta_c = 0$, suggesting that arbitrarily weak η terms will gap out the surface Bogoliubov-Dirac cones. Focusing on the small momentum region, the surface Hamiltonian in Eq. (4) can be simplified by neglecting the cubic-order momentum terms as

$$H_s(k_y, k_z) = -\frac{\tilde{m}\eta}{t} k_z \tau_z s_y + \frac{\Delta_s}{2} (R_{\text{BIS}}^2 - R_{\text{PNS}}^2 - \frac{t_z}{t} k_z^2) \tau_y s_y + \lambda k_y s_z. \quad (5)$$

When $\eta \neq 0$ and $R_{\text{BIS}} > R_{\text{PNS}}$, the first line realizes a one-dimensional (1D) time-reversal invariant TSC in the k_z direction¹¹⁵. Considering a half-infinity surface occupying the region $0 \leq z < +\infty$, doing the replacement $k_z \rightarrow -i\partial_z$ and solving the eigenvalue equation $H_s\phi_\alpha(z) = E_\alpha\phi_\alpha(z)$ under boundary conditions $\phi_\alpha(0) = \phi_\alpha(+\infty) = 0$, one will find the existence of two branches of charge-neutral midgap states with opposite spin polarizations on the boundary of the surface, with their dispersions given by $E_{\alpha=1,2} = \pm\lambda k_y$ (see Appendix A), indicating the appearance of helical Majorana modes on the hinges. In Fig. 3, we further provide numerical results for $\mu \neq 0$ to support the realization of a second-order time-reversal invariant TSC with helical Majorana hinge modes when the criterion established above is fulfilled.

IV. FIRST-ORDER TIME-REVERSAL INVARIANT TOPOLOGICAL SUPERCONDUCTIVITY IN THIN-FILM SUPERCONDUCTING DIRAC SEMIMETALS

For s_{\pm} -wave pairing, we have shown that the first-order topology is always trivial when time-reversal symmetry and inversion symmetry are preserved simultaneously. In the following, we consider reducing the bulk

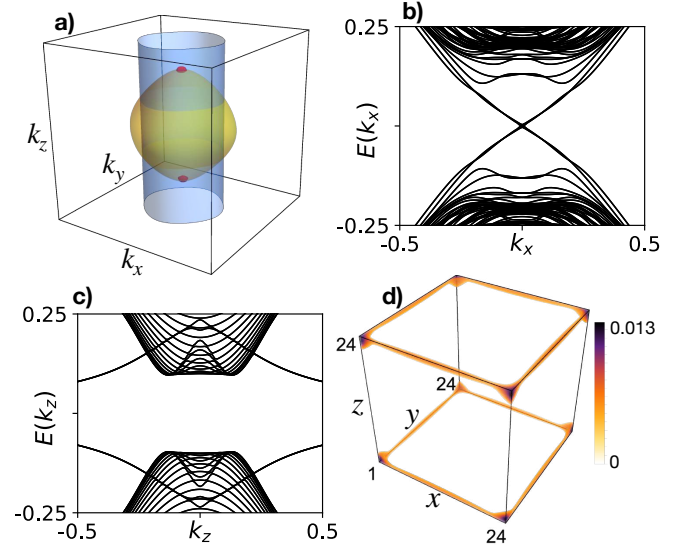


FIG. 3. (Color online) Chosen parameters are $m = 3$, $t = t_z = 2$, $\lambda = \eta = 1$, $\mu = 0.2$, and $\Delta_0 = \Delta_s = 0.2$. (a) The PNS (blue), the BIS (yellow), and the two Fermi surfaces (red). (b) Helical Majorana hinge modes along the x direction. Both y and z directions have open boundary conditions with $N_y = N_z = 60$ lattice sites. (c) No gapless hinge modes along the z direction. Both x and y directions have open boundary conditions with $N_x = N_y = 50$. (d) The probability density distribution of the four eigenstates whose energies are in the middle of the BdG energy spectrum, confirming the localization of the helical Majorana modes on the hinges. All three directions have open boundary conditions with $N_x = N_y = N_z = 24$.

superconducting DSM to a thin film along the z direction so that inversion symmetry can be easily broken by applying a gate voltage to the top and bottom layers¹¹⁶. Remarkably, we find that when $\eta \neq 0$, a first-order time-reversal invariant TSC can be achieved (a discussion of the $\eta = 0$ case is provided in Appendix B). It is worth noting that although the thin-film superconducting DSM still belongs to class DIII, the classification of the gapped phases is changed from \mathbb{Z} to \mathbb{Z}_2 due to the dimensional reduction, with the \mathbb{Z}_2 invariant given in the weak-pairing limit by¹¹²

$$N_{2D} = \prod_i [\text{sgn}(\Delta_i)]^{m_i}. \quad (6)$$

Here, m_i counts the number of time-reversal invariant momenta enclosed by the i th Fermi surface, and $N_{2D} = -1$ indicates the realization of a first-order time-reversal invariant TSC with helical Majorana edge modes^{110,116–121}.

To be specific, here we consider the number of layers to be $N_z = 5$ and add a potential profile of the form $V(z)\psi_{k_x, k_y, z}^\dagger \psi_{k_x, k_y, z}$ to the BdG Hamiltonian, where $V(z) = V_0(2z - N_z - 1)/(N_z - 1)$ with $z = 1, 2, \dots, N_z$, *i.e.* the gate voltage varies linearly across the sample, so the voltage difference between top and bottom layers is $2V_0$.

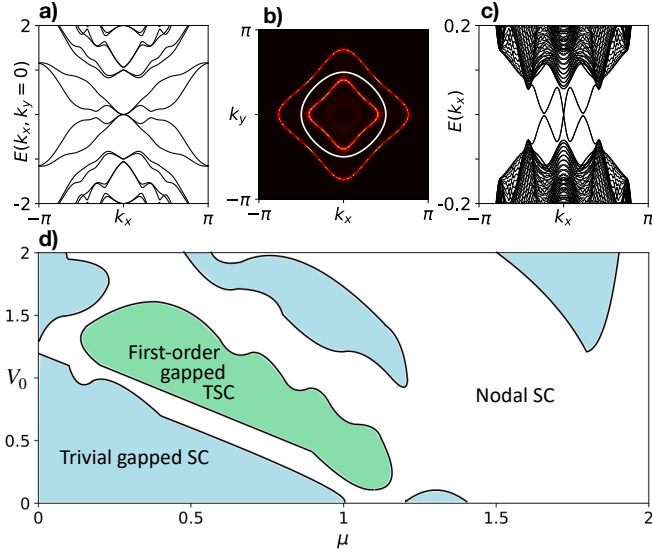


FIG. 4. (Color online) Chosen parameters are $m = 3$, $t = t_z = 2$, $\lambda = \eta = 1$, and $N_z = 5$. a) The normal-state energy spectrum along the $k_y = 0$ line at $V_0 = 1$. b) The configurations of pairing line node (white) and Fermi surfaces (red) in the two-dimensional Brillouin zone for $\Delta_0 = \Delta_s = 0.2$, $\mu = 0.7$ and $V_0 = 1$. c) With the same set of parameters as in b), the energy spectrum shows the existence of \mathbb{Z}_2 nontrivial helical Majorana modes in the gap when open boundary conditions are taken in both y and z directions with $N_y = 100$. The two tiny gaps at finite momentum are intrinsic and correspond to avoided crossings. d) The phase diagram includes three topologically distinct phases.

With the same set of parameters as in the bulk case, the corresponding normal-state energy spectra for the thin film are shown in Fig. 4(a). One finds that, in this case, the normal state is a two-dimensional semimetal with spin-split dispersion (away from time-reversal invariant momenta). Assuming the location of PNS to be fixed, we find that tuning the chemical potential can make the PNS fall between two disconnected Fermi surfaces, as shown in Fig. 4(b). In accordance with Eq. (6), it is readily found that N_{2D} takes the nontrivial value -1 for the configuration in Fig. 4(b). By numerically calculating the energy spectra in a cylinder geometry, the existence of robust midgap helical Majorana edge modes confirms the realization of a first-order time-reversal invariant TSC, as shown in Fig. 4(c). Moreover, the phase diagram in Fig. 4(d) shows that, for a broad regime of μ , the thin-film superconducting DSM can be made topologically nontrivial by tuning the gate voltage.

V. DISCUSSION AND CONCLUSION

We have uncovered topological criteria for the realization of surface Bogoliubov-Dirac cones and helical Majorana hinge modes in three-dimensional superconducting DSMs with s_{\pm} -wave pairing. Remarkably, the

topological criteria admit a simple geometric interpretation in terms of the relative configurations of BIS, PNS, and Fermi surface. We have also shown that first-order time-reversal invariant TSCs can be realized in thin-film superconducting DSMs by applying a gate voltage to break inversion symmetry. Our work suggests that intrinsic superconductors simultaneously hosting a gapless Dirac band structure and unconventional superconductivity can realize a diversity of intrinsic time-reversal invariant TSCs and Majorana modes. Our predictions can be tested in iron-based superconductors such as $\text{LiFe}_{1-x}\text{Co}_x\text{As}$ ⁸⁶ by adjusting the doping level so as to position the Fermi energy near the bulk Dirac points. Experimentally, the surface Bogoliubov-Dirac cones can be detected by angle-resolved photoemission spectroscopy^{85,86}, and the helical Majorana modes can be measured by scanning tunneling microscopy¹²² as well as contact methods¹²³.

ACKNOWLEDGMENTS

M.Kh. and J.M. acknowledge support from NSERC Discovery Grant No. RGPIN-2020-06999. J.M. also acknowledges support from NSERC Discovery Grant No. RGPAS-2020-00064; the CRC Program; CIFAR; a Government of Alberta MIF Grant; a Tri-Agency NFRF Grant (Exploration Stream); and the PIMS CRG program. Z.-Y.Z. and Z.Y. are supported by the National Natural Science Foundation of China (Grants No. 11904417 and 12174455) and the Natural Science Foundation of Guangdong Province (Grant No. 2021B1515020026).

Appendix A: Derivation of the low-energy Hamiltonian for the surface states

We start with the full Bogoliubov-de Gennes (BdG) lattice Hamiltonian, which reads

$$\begin{aligned}
 H_{\text{BdG}}(\mathbf{k}) = & [m - t(\cos k_x + \cos k_y) - t_z \cos k_z] \tau_z \sigma_z \\
 & + \lambda(\sin k_x s_z \sigma_x - \sin k_y \tau_z \sigma_y) - \mu \tau_z \\
 & + \eta \sin k_z (\cos k_x - \cos k_y) s_x \sigma_x \\
 & + 2\eta \sin k_x \sin k_y \sin k_z \tau_z s_y \sigma_x \\
 & + [\Delta_0 - \Delta_s (\cos k_x + \cos k_y)] \tau_y s_y, \quad (\text{A1})
 \end{aligned}$$

where the Pauli matrices σ_i , s_i , and τ_i act on the orbital, spin, and particle-hole degrees of freedom, respectively. Similar to the main text, the lattice constants are set to unity and the identity matrices are made implicit for brevity. To derive the low-energy Hamiltonian for the surface states, without loss of generality, we consider that the band inversion surface (BIS) only encloses one time-reversal invariant momentum, $\Gamma = (0, 0, 0)$. Accordingly, we expand the lattice Hamiltonian around Γ to obtain the corresponding continuum bulk Hamiltonian, which

reads

$$\begin{aligned}
H_c(\mathbf{k}) = & \left[\tilde{m} + \frac{t}{2}(k_x^2 + k_y^2) + \frac{t_z}{2}k_z^2 \right] \tau_z \sigma_z \\
& + \lambda(k_x s_z \sigma_x - k_y \tau_z \sigma_y) - \mu \tau_z \\
& - \frac{\eta}{2}k_z(k_x^2 - k_y^2)s_x \sigma_x + 2\eta k_z k_x k_y \tau_z s_y \sigma_x \\
& + \left[\tilde{\Delta} + \frac{\Delta_s}{2}(k_x^2 + k_y^2) \right] \tau_y s_y, \quad (\text{A2})
\end{aligned}$$

where $\tilde{m} = m - 2t - t_z$ and $\tilde{\Delta} = \Delta_0 - 2\Delta_s$. Before proceeding, it is worth noting that while the low-energy bulk physics is dominated by the gapless bulk Dirac cones, one cannot use the low-energy bulk Hamiltonian expanded around the Dirac points to extract the low-energy boundary Hamiltonian describing the surface states; instead, one needs to use the low-energy bulk Hamiltonian expanded around the band inversion momentum (above we have assumed it to be Γ). The surface states originate from the band inversion, so one should expand around the band inversion momentum to take into account the full band inversion region. On the other hand, the locations of Dirac points correspond to the boundary of the band inversion surface along the rotation-symmetric axis, so in fact one cannot obtain the surface-state information through the low-energy Hamiltonian expanded around the Dirac points. In addition, it is also worth noting that we have only kept the leading term in momentum for each term in the continuum bulk Hamiltonian for simplicity. Such an approximation allows a simple analytic derivation of the low-energy boundary Hamiltonian, and it captures the essential physics quite accurately, particularly in the regime close to the band inversion momen-

tum.

To be specific, in the following we assume $\{t, t_z, \lambda, \eta\}$ to be all positive and \tilde{m} to be negative so that the normal state harbors a pair of Dirac points at $(0, 0, \pm\sqrt{-2\tilde{m}/t_z})$. For the pairing order parameter, we assume $\Delta_s > 0$ but $\tilde{\Delta} < 0$, so that the pairing amplitude has a nodal surface in momentum space. For later discussion, we will introduce two quantities, $R_{\text{BIS}} = \sqrt{-2\tilde{m}/t}$ and $R_{\text{PNS}} = \sqrt{-2\tilde{\Delta}/\Delta_s}$, which correspond to the radius of the ellipsoidal BIS in the $k_z = 0$ plane and the radius of the cylindrical pairing node surface (PNS), respectively. Geometrically, when $0 < R_{\text{PNS}} < R_{\text{BIS}}$, the BIS and PNS intersect.

We will focus on side surfaces which can harbor both Fermi arcs and Dirac cones. Since the Hamiltonian has C_{4z} -rotation symmetry, we can just focus on the x -normal surface. To be specific, we consider that the system occupies the region $0 \leq x < +\infty$. Since the presence of a boundary breaks the translation symmetry in the x direction, k_x needs to be replaced by $-i\partial_x$. Accordingly, we have

$$\begin{aligned}
H_c(-i\partial_x, k_y, k_z) = & \left(\tilde{m} - \frac{t}{2}\partial_x^2 + \frac{t}{2}k_y^2 + \frac{t_z}{2}k_z^2 \right) \tau_z \sigma_z \\
& - i\lambda\partial_x s_z \sigma_x - \lambda k_y \tau_z \sigma_y - \mu \tau_z \\
& + \frac{\eta}{2}k_z(\partial_x^2 + k_y^2)s_x \sigma_x - 2i\eta k_z k_y \partial_x \tau_z s_y \sigma_x \\
& + \left(\tilde{\Delta} + \frac{\Delta_s}{2}k_y^2 - \frac{\Delta_s}{2}\partial_x^2 \right) \tau_y s_y. \quad (\text{A3})
\end{aligned}$$

In the next step, we decompose the Hamiltonian into two parts, *i.e.*, $H_c = H_0 + H'$, with

$$H_0(-i\partial_x, k_y, k_z) = \left(\tilde{m} - \frac{t}{2}\partial_x^2 + \frac{t}{2}k_y^2 + \frac{t_z}{2}k_z^2 \right) \tau_z \sigma_z - i\lambda\partial_x s_z \sigma_x - \lambda k_y \tau_z \sigma_y, \quad (\text{A4})$$

$$H'(-i\partial_x, k_y, k_z) = \frac{\eta}{2}k_z(\partial_x^2 + k_y^2)s_x \sigma_x - 2i\eta k_z k_y \partial_x \tau_z s_y \sigma_x - \mu \tau_z + \left(\tilde{\Delta} + \frac{\Delta_s}{2}k_y^2 - \frac{\Delta_s}{2}\partial_x^2 \right) \tau_y s_y, \quad (\text{A5})$$

where H_0 is the part describing the Dirac semimetal without the cubic-order terms. It is worth noting that we always put the terms with the same Pauli matrices together as they play the same role. Moreover, as the pairing constants are much smaller than the hopping constants in materials and as the regime in which the chemical potential is close to the Dirac points is of particular interest, *i.e.*, $\mu \rightarrow 0$, we will treat all terms in H' as perturbations. In the following, we first solve the equation $H_0\psi_\alpha(x) = E_\alpha\psi_\alpha(x)$. For surface states localized on the $x = 0$ surface, we demand that their wave functions satisfy the boundary conditions $\psi_\alpha(0) = \psi_\alpha(\infty) = 0$. It is readily found that there are four solutions, with two solutions corresponding to $E_\alpha = \lambda k_y$ and the other two corresponding to $E_\alpha = -\lambda k_y$. The expressions for the

four solutions can be compactly written as²⁴

$$\psi_\alpha = \mathcal{N} \sin(\kappa_1 x) e^{-(\kappa_2 x)} e^{ik_y y} e^{ik_z z} \chi_\alpha, \quad (\text{A6})$$

where the normalization constant is given by $\mathcal{N} = 2\sqrt{\kappa_2(\kappa_1^2 + \kappa_2^2)}/\kappa_1^2$, with

$$\kappa_1 = \sqrt{\frac{-2\tilde{m} - tk_y^2 - t_z k_z^2}{t} - \left(\frac{\lambda}{t}\right)^2}, \quad (\text{A7})$$

$$\kappa_2 = \frac{\lambda}{t}. \quad (\text{A8})$$

The spinor χ_α satisfies $\tau_z s_z \sigma_y \chi_\alpha = -\chi_\alpha$. Here, without loss of generality, we choose $\chi_1 = |\tau_z = 1, s_z = 1, \sigma_y = -1\rangle$, $\chi_2 = |\tau_z = 1, s_z = -1, \sigma_y = 1\rangle$, $\chi_3 = |\tau_z = -1, s_z = 1, \sigma_y = 1\rangle$ and $\chi_4 = |\tau_z = -1, s_z = -1, \sigma_y = -1\rangle$.

The normalization of the wave functions suggests that the boundary modes exist only when $(\kappa_1^2 + \kappa_2^2) > 0$, *i.e.* $tk_y^2 + t_z k_z^2 < -2\tilde{m}$, which is just the projection of BIS in the k_x direction. In the basis $(\psi_1, \psi_2, \psi_3, \psi_4)^T$, the surface-state Hamiltonian contributed by H_0 reads

$$H_s^{(0)}(k_y, k_z) = \lambda k_y s_z, \quad (\text{A9})$$

which only leads to straight Fermi arcs. For notational simplicity, we still make the identity matrix implicit. Taking into account H' , its contribution can be deter-

mined by the standard perturbation theory,

$$[H'_s(k_y, k_z)]_{\alpha\beta} = \int_0^\infty \psi_\alpha^\dagger(x) H'(-i\partial_x, k_y, k_z) \psi_\beta(x) dx. \quad (\text{A10})$$

In terms of the Pauli matrices, one finds

$$H'_s(k_y, k_z) = v_z(k_y, k_z) k_z \tau_z s_y - \mu \tau_z + \left(\tilde{\Delta} - \frac{\Delta_s \tilde{m}}{t} - \frac{\Delta_s t_z}{2t} k_z^2\right) \tau_y s_y \quad (\text{A11})$$

with¹⁰⁰

$$\begin{aligned} v_z(k_y, k_z) &= -\mathcal{N}^2 \int_0^\infty \sin(\kappa_1 x) e^{-(\kappa_2 x)} \frac{\eta}{2} (\partial_x^2 + k_y^2) \sin(\kappa_1 x) e^{-(\kappa_2 x)} dx \\ &= -\frac{\eta}{t} (\tilde{m} + tk_y^2 + t_z k_z^2/2). \end{aligned} \quad (\text{A12})$$

Putting the two parts together, the low-energy Hamiltonian describing the surface states on the $x = 0$ surface has the form

$$\begin{aligned} H_s(k_y, k_z) &= H_s^0 + H'_s \\ &= \lambda k_y s_z + v_z(k_y, k_z) k_z \tau_z s_y - \mu \tau_z \\ &\quad + \left(\tilde{\Delta} - \frac{\Delta_s \tilde{m}}{t} - \frac{\Delta_s t_z}{2t} k_z^2\right) \tau_y s_y. \end{aligned} \quad (\text{A13})$$

It is readily found that the boundary Hamiltonian preserves all nonspatial symmetries of the bulk Hamiltonian, including the time-reversal symmetry ($\mathcal{T} = is_y \mathcal{K}$), particle-hole symmetry ($\mathcal{P} = \tau_x \mathcal{K}$), and their combination, the chiral symmetry ($\mathcal{C} = \tau_x s_y$).

Next, let us rewrite the Hamiltonian as

$$\begin{aligned} H_s(k_y, k_z) &= \lambda k_y s_z + v_z(k_y, k_z) k_z \tau_z s_y - \mu \tau_z \\ &\quad + \frac{\Delta_s}{2} \left(\frac{2\tilde{\Delta}}{\Delta_s} - \frac{2\tilde{m}}{t} - \frac{t_z}{t} k_z^2 \right) \tau_y s_y \\ &= \lambda k_y s_z + v_z(k_y, k_z) k_z \tau_z s_y - \mu \tau_z \\ &\quad + \frac{\Delta_s}{2} \left(R_{\text{BIS}}^2 - R_{\text{PNS}}^2 - \frac{t_z}{t} k_z^2 \right) \tau_y s_y, \end{aligned} \quad (\text{A14})$$

which is Eq. (4). When $\eta = 0$, the Hamiltonian reduces to

$$\begin{aligned} H_s(k_y, k_z) &= \lambda k_y s_z - \mu \tau_z \\ &\quad + \frac{\Delta_s}{2} \left(R_{\text{BIS}}^2 - R_{\text{PNS}}^2 - \frac{t_z}{t} k_z^2 \right) \tau_y s_y. \end{aligned} \quad (\text{A15})$$

At $\mu = 0$, one can find that there are two cones with linear dispersion and double degeneracy at $(k_y, k_z) = (0, \pm \sqrt{\frac{t}{t_z} (R_{\text{BIS}}^2 - R_{\text{PNS}}^2)})$. Since the Hamiltonian can be decomposed into two decoupled parts when $\mu = 0$, it is easy to see that the Bogoliubov quasiparticle operators will take the form $\gamma_{\mathbf{k},1} = u_{\mathbf{k},1} c_{\mathbf{k},\uparrow} + v_{\mathbf{k},1} c_{-\mathbf{k},\downarrow}^\dagger$

or $\gamma_{\mathbf{k},2} = u_{\mathbf{k},2} c_{\mathbf{k},\downarrow} + v_{\mathbf{k},2} c_{-\mathbf{k},\uparrow}^\dagger$ (the concrete expressions for $u_{\mathbf{k},1(2)}$ and $v_{\mathbf{k},1(2)}$ are not important here). In each case, the quasiparticle operators do not satisfy the self-conjugate property $\gamma_{\mathbf{k},1(2)} \neq \gamma_{-\mathbf{k},1(2)}^\dagger$ as the electron part and hole part have opposite spin polarizations. Therefore we dub these cones with linear dispersion as Bogoliubov-Dirac cones to distinguish them from Majorana cones. Recall that the gapless surface states only exist within the regime satisfying $tk_y^2 + t_z k_z^2 < -2\tilde{m}$, *i.e.* $k_y^2 + \frac{t_z}{t} k_z^2 < R_{\text{BIS}}^2$. Therefore, the condition for the existence of Bogoliubov-Dirac cones at $\mu = 0$ is very simple. That is, $0 < R_{\text{PNS}} < R_{\text{BIS}}$. Geometrically, this corresponds to the BIS and PNS intersecting in momentum space. Once $\mu \neq 0$, the double degeneracy of the Bogoliubov-Dirac cones at $\mu = 0$ is split, and there are four separated Bogoliubov-Dirac cones, with their locations being at $(k_y, k_z) = (\pm\mu/\lambda, \pm\sqrt{\frac{t}{t_z} (R_{\text{BIS}}^2 - R_{\text{PNS}}^2)})$. Since the Bogoliubov-Dirac cones must exist in the regime satisfying $k_y^2 + \frac{t_z}{t} k_z^2 < R_{\text{BIS}}^2$, the condition for their existence becomes $|\frac{\mu}{\lambda}| < R_{\text{PNS}} < R_{\text{BIS}}$. Interestingly, $|\frac{\mu}{\lambda}|$ also has a geometric interpretation. To see this, let us focus on the normal state and investigate the bulk Fermi surface. When $\eta = 0$, the energy spectrum for the normal state is

$$E(\mathbf{k}) = \pm \sqrt{\lambda^2 (k_x^2 + k_y^2) + M^2(\mathbf{k})} \quad (\text{A16})$$

where $M(\mathbf{k}) = \tilde{m} + \frac{t}{2} (k_x^2 + k_y^2) + \frac{t_z}{2} k_z^2$. The bulk Fermi surface is determined by

$$\lambda^2 (k_x^2 + k_y^2) + M^2(\mathbf{k}) = \mu^2 \quad (\text{A17})$$

It is readily found that the maximum radius of the Fermi surface in the k_x - k_y plane is equal to $|\frac{\mu}{\lambda}|$. Defining $R_{\text{FS}} = |\frac{\mu}{\lambda}|$, the criterion for the existence of surface Bogoliubov-Dirac cones can be rewritten as $R_{\text{FS}} < R_{\text{PNS}} < R_{\text{BIS}}$. This form describes a very simple geometric picture. That is, the PNS encloses the bulk Fermi surface and simultaneously intersects the BIS. Before ending

this part, let us further give a discussion of the topological protection of the surface Bogoliubov-Dirac cones. As we mentioned above, the two-dimensional boundary Hamiltonian inherits the chiral symmetry from the three-dimensional bulk. Due to the existence of chiral symmetry, the band touching points of the surface energy spectrum can be assigned a winding number to characterize their topology. First, one can change the basis so that the chiral operator takes a diagonal form in the new basis. Accordingly, it is known that the Hamiltonian will become off-diagonal, with the form

$$\tilde{H}(k_y, k_z) = \begin{pmatrix} 0 & Q(k_y, k_z) \\ Q^\dagger(k_y, k_z) & 0 \end{pmatrix}, \quad (\text{A18})$$

where $Q(k_y, k_z)$ is a 2×2 matrix, with its elements $Q_{11} =$

$Q_{22} = \lambda k_y$, $Q_{12} = i\mu - iv_z(k_y, k_z)k_z + \frac{\Delta_s}{2}(R_{\text{BIS}}^2 - R_{\text{PNS}}^2 - \frac{t_z}{t}k_z^2)$, and $Q_{21} = -i\mu - iv_z(k_y, k_z)k_z - \frac{\Delta_s}{2}(R_{\text{BIS}}^2 - R_{\text{PNS}}^2 - \frac{t_z}{t}k_z^2)$. When a closed path is chosen to enclose one band touching point of the surface energy spectrum, a winding number can be defined to characterize the band touching point in accordance with the below formula:¹¹⁴

$$\omega = \frac{i}{2\pi} \oint_C \text{Tr}[Q^{-1} \partial_k Q] dk. \quad (\text{A19})$$

The topological nature of the winding number guarantees the robustness of separated band touching points. As a result, one gapless Bogoliubov-Dirac cone can be gapped only when it meets another gapless Bogoliubov-Dirac cone characterized by an opposite winding number.

Now let us consider $\eta \neq 0$. Accordingly, the surface energy spectrum becomes

$$E(k_y, k_z) = \pm \sqrt{\left(\sqrt{\lambda^2 k_y^2 + v_z^2(k_y, k_z)k_z^2} \pm \mu \right)^2 + \frac{\Delta_s^2}{4} \left(R_{\text{BIS}}^2 - R_{\text{PNS}}^2 - \frac{t_z}{t}k_z^2 \right)^2}. \quad (\text{A20})$$

The surface Bogoliubov-Dirac cones, if they remain, are located at a value of $k_z = \pm \sqrt{t(R_{\text{BIS}}^2 - R_{\text{PNS}}^2)/t_z}$ independent of η . The k_y value needs to be determined by solving the equation

$$\lambda^2 k_y^2 + \eta^2 (k_y^2 + \tilde{\Delta}/\Delta_s)^2 t (R_{\text{BIS}}^2 - R_{\text{PNS}}^2)/t_z = \mu^2, \quad (\text{A21})$$

or in the standard form

$$\begin{aligned} & [\eta^2 t (R_{\text{BIS}}^2 - R_{\text{PNS}}^2)/t_z] k_y^4 \\ & + [\lambda^2 + 2\eta^2 (\tilde{\Delta}/\Delta_s) t (R_{\text{BIS}}^2 - R_{\text{PNS}}^2)/t_z] k_y^2 \\ & + \eta^2 (\tilde{\Delta}/\Delta_s)^2 t (R_{\text{BIS}}^2 - R_{\text{PNS}}^2)/t_z - \mu^2 = 0. \end{aligned} \quad (\text{A22})$$

By defining

$$a \equiv [\eta^2 t (R_{\text{BIS}}^2 - R_{\text{PNS}}^2)/t_z], \quad (\text{A23})$$

$$b \equiv [\lambda^2 + 2\eta^2 (\tilde{\Delta}/\Delta_s) t (R_{\text{BIS}}^2 - R_{\text{PNS}}^2)/t_z], \quad (\text{A24})$$

$$c \equiv \eta^2 (\tilde{\Delta}/\Delta_s)^2 t (R_{\text{BIS}}^2 - R_{\text{PNS}}^2)/t_z - \mu^2, \quad (\text{A25})$$

it is known that the solutions for k_y^2 take the standard form

$$k_y^2 = \frac{-b \pm \sqrt{b^2 - 4ac}}{2a}. \quad (\text{A26})$$

There will exist gapless Bogoliubov-Dirac cones in the surface Brillouin zone as long as real and positive solutions for k_y^2 exist. As we are interested in the movements of the Bogoliubov-Dirac cones with the increase in η from 0, in the following we focus on the case with $b > 0$ to give a discussion. As here the parameter a is positive, the existence of a physical solution then requires $c < 0$. Accordingly, one can find that the condition for the existence of gapless Bogoliubov-Dirac cones is

$$\begin{aligned} |\eta| < \eta_c &= \frac{|\mu| \Delta_s}{|\tilde{\Delta}|} \sqrt{\frac{t_z}{t(R_{\text{BIS}}^2 - R_{\text{PNS}}^2)}} \\ &= \frac{2|\mu|}{R_{\text{PNS}}^2} \sqrt{\frac{t_z}{t(R_{\text{BIS}}^2 - R_{\text{PNS}}^2)}}. \end{aligned} \quad (\text{A27})$$

Putting η_c back into the formula for b , one obtains

$$b = \lambda^2 + 2\mu^2 \frac{\Delta_s}{\tilde{\Delta}}. \quad (\text{A28})$$

As long as the chemical potential $|\mu| < \mu_c = \sqrt{|\frac{\tilde{\Delta}}{2\Delta_s}|} \lambda$, the parameter b is positive, and the above formula for η_c is valid. To intuitively see the effect of η terms on k_y^2 , we consider $|\mu| < \mu_c$ and η to be small so that we can do an expansion in η . To second order, we find

$$k_y^2 \approx \frac{\mu^2}{\lambda^2} - \frac{\eta^2}{\lambda^2} \frac{t}{t_z} (R_{\text{BIS}}^2 - R_{\text{PNS}}^2) \left(\frac{\tilde{\Delta}}{\Delta_s} \right)^2 \left[1 + \frac{\mu^2}{\lambda^2} \frac{\Delta_s}{\tilde{\Delta}} \right]. \quad (\text{A29})$$

In the weakly doped regime, $\mu \ll \lambda$, one can see

that the η terms decrease the separation of surface

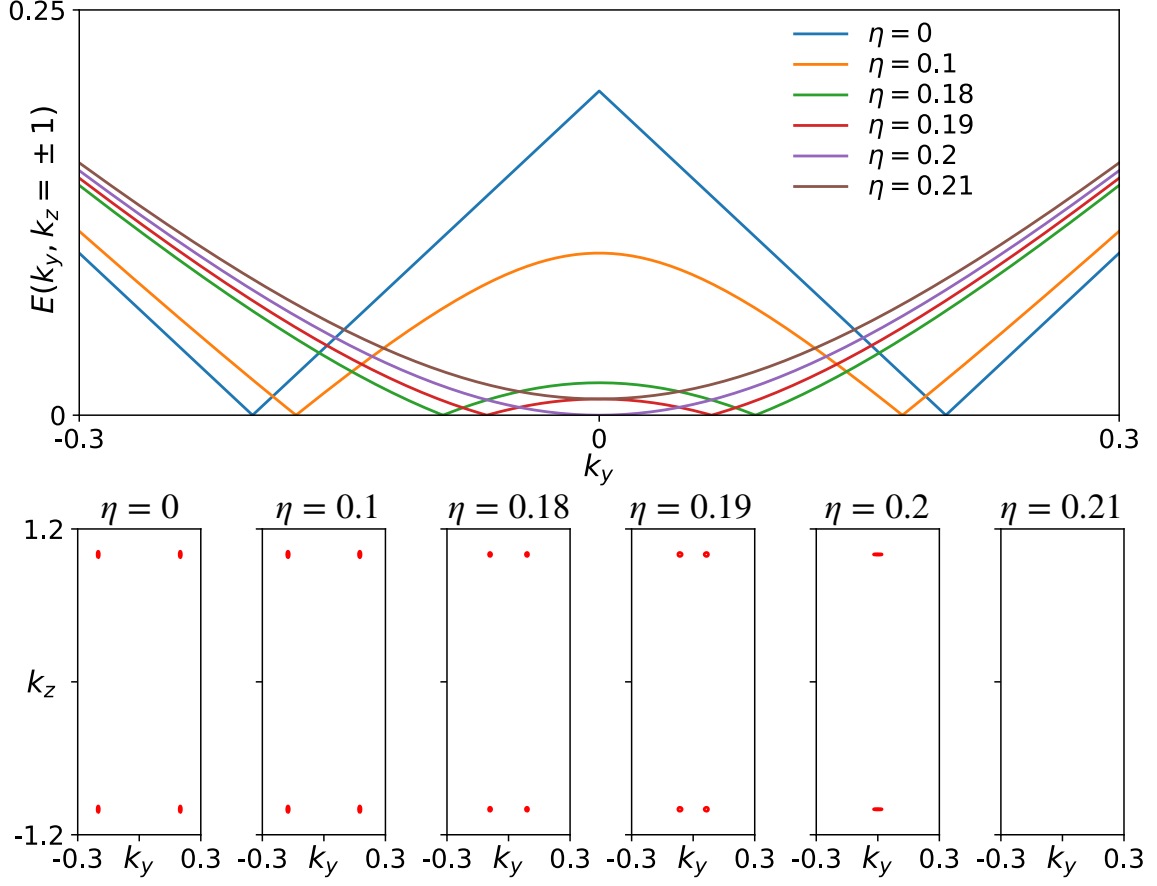


FIG. A1. (Color online) Chosen parameters are $m = 3$, $t = t_z = 2$, $\lambda = 1$, $\mu = 0.2$, and $\Delta_0 = \Delta_s = 0.2$. Accordingly, $R_{\text{BIS}} = \sqrt{3}$, $R_{\text{PNS}} = \sqrt{2}$, and $\eta_c = 0.2$. The x -normal surface band structure at $k_z = \pm 1$ given by Eq. (A14) (top panel) and the position of four surface Bogoliubov-Dirac cones (bottom panels) for different values of η . As expected, only the k_y coordinate of the position of the surface Bogoliubov-Dirac cones depends on η . Pairwise annihilation of the cones occurs at the critical value $\eta = 0.2$.

Bogoliubov-Dirac cones in the k_y direction, consistent with the picture that the surface Bogoliubov-Dirac cones will annihilate each other when η is larger than a critical value. In Fig. A1, we show the evolution of the positions of surface Bogoliubov-Dirac cones with respect to η explicitly. According to this evolution, one can find that the value at which the surface Bogoliubov-Dirac cones merge in pairs agrees with the formula for η_c in Eq. (A27). By diagonalizing the full lattice Hamiltonian with open boundary conditions in the x direction, we find that the locations and evolution of surface Bogoliubov-Dirac cones on the x -normal surface agree well with the analytical analysis above, as shown in Fig. A2.

After gapping out the surface Bogoliubov-Dirac cones, we have shown both analytically and numerically that one-dimensional propagating helical Majorana modes will emerge on the hinges of a cubic sample. Here, we provide more details about the analytical derivation of the low-energy Hamiltonian for the helical Majorana hinge modes at the limit $\mu = 0$. At $\mu = 0$, the surface-state

Hamiltonian becomes

$$H_s(k_y, k_z) = \lambda k_y s_z - \frac{\eta k_z}{t} (\tilde{m} + t k_y^2 + t_z k_z^2 / 2) \tau_z s_y + \frac{\Delta_s}{2} (R_{\text{BIS}}^2 - R_{\text{PNS}}^2 - \frac{t_z}{t} k_z^2) \tau_y s_y. \quad (\text{A30})$$

It is readily found that the energy spectrum for this Hamiltonian is fully gapped as long as $\eta \neq 0$ and $R_{\text{BIS}} \neq R_{\text{PNS}}$. Let us focus on the small-momentum region; accordingly, we will only keep the leading momentum terms in each term of the surface-state Hamiltonian. Then the Hamiltonian reduces to

$$H_s(k_y, k_z) = \lambda k_y s_z - \frac{\eta \tilde{m} k_z}{t} \tau_z s_y + \frac{\Delta_s}{2} (R_{\text{BIS}}^2 - R_{\text{PNS}}^2 - \frac{t_z}{t} k_z^2) \tau_y s_y. \quad (\text{A31})$$

If the open boundary condition is further taken in the z

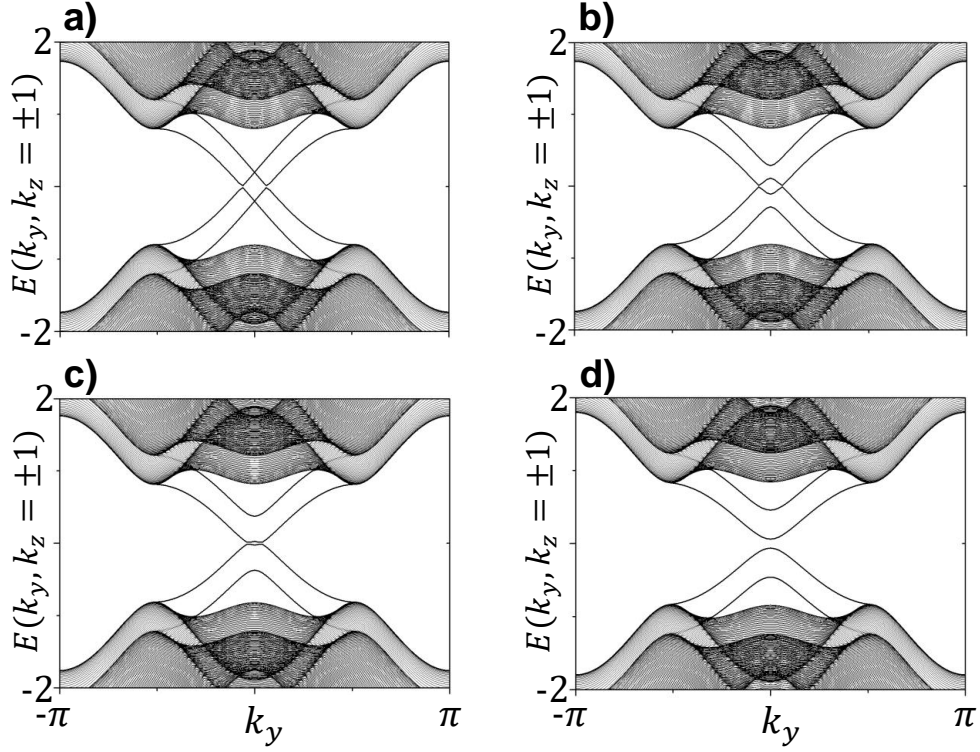


FIG. A2. Energy spectrum of the full lattice Hamiltonian under open boundary conditions in the x direction and periodic boundary conditions in the y and z directions. Chosen parameters are $m = 3$, $t = t_z = 2$, $\lambda = 1$, $\mu = 0.2$, and $\Delta_0 = \Delta_s = 0.2$. a) $\eta = 0$, b) $\eta = 0.1$, c) $\eta = 0.2$, d) $\eta = 0.3$.

direction, then the Hamiltonian becomes

$$H_s(k_y, -i\partial_z) = \lambda k_y s_z + i \frac{\eta \tilde{m}}{t} \tau_z s_y \partial_z + \frac{\Delta_s}{2} (R_{\text{BIS}}^2 - R_{\text{PNS}}^2 + \frac{t_z}{t} \partial_z^2) \tau_y s_y. \quad (\text{A32})$$

As the Hamiltonian takes a form similar to H_0 in Eq. (A4), one can easily find that if we consider a half-infinity sample with the boundary at $z = 0$ (the boundary is in fact a hinge as it corresponds to the boundary of a surface), there exist two solutions satisfying the eigenvalue equation $H_s \phi_\alpha(z) = E_\alpha \phi_\alpha(z)$ and the boundary condition $\phi_\alpha(0) = \phi_\alpha(\infty) = 0$. The expressions for the two solutions are similar to those in Eq. (A6),

$$\phi_\alpha(z) = \mathcal{N}' \sin(\kappa'_1 z) e^{-(\kappa'_2 z)} e^{ik_y y} \chi'_\alpha, \quad (\text{A33})$$

where the normalization constant is given by $\mathcal{N}' = 2\sqrt{\kappa'_2(\kappa'^2_1 + \kappa'^2_2)/\kappa'^2_1}$, with

$$\kappa'_1 = \sqrt{\frac{t(R_{\text{BIS}}^2 - R_{\text{PNS}}^2)}{t_z} - \left(\frac{\eta \tilde{m}}{t_z \Delta_s}\right)^2}, \quad (\text{A34})$$

$$\kappa'_2 = -\frac{\eta \tilde{m}}{t_z \Delta_s}. \quad (\text{A35})$$

The normalization of the wave functions requires $R_{\text{BIS}}^2 > R_{\text{PNS}}^2$, indicating that the crossing of the BIS and PNS is

a precondition for the realization of the helical Majorana hinge modes. Here the two spinors χ'_α can be chosen as $\chi'_1 = |\tau_x = 1, s_z = 1\rangle$ and $\chi'_2 = |\tau_x = 1, s_z = -1\rangle$. Correspondingly, $E_1 = \lambda k_y$ and $E_2 = -\lambda k_y$. As the two spinors indicate that each branch of the hinge states is spin-polarized and an equal superposition of electron and hole, this analysis confirms that the two branches of hinge states correspond to a pair of helical Majorana modes. In the basis $(\phi_1, \phi_2)^T$, the low-energy Hamiltonian that describes the helical Majorana hinge modes reads

$$H_h(k_y) = \lambda k_y s_z. \quad (\text{A36})$$

Appendix B: Importance of η terms for the realization of first-order time-reversal invariant topological superconductivity in thin films of superconducting Dirac semimetal

In this appendix, we will show that the η terms are also crucial for the realization of first-order time-reversal invariant topological superconductivity in thin films of the superconducting Dirac semimetal. Before proceeding, we recall the fact that, for the even-parity pairing discussed here, lifting the spin degeneracy of the Fermi surface is a precondition for the realization of first-order time-reversal invariant topological superconductivity in two dimensions.

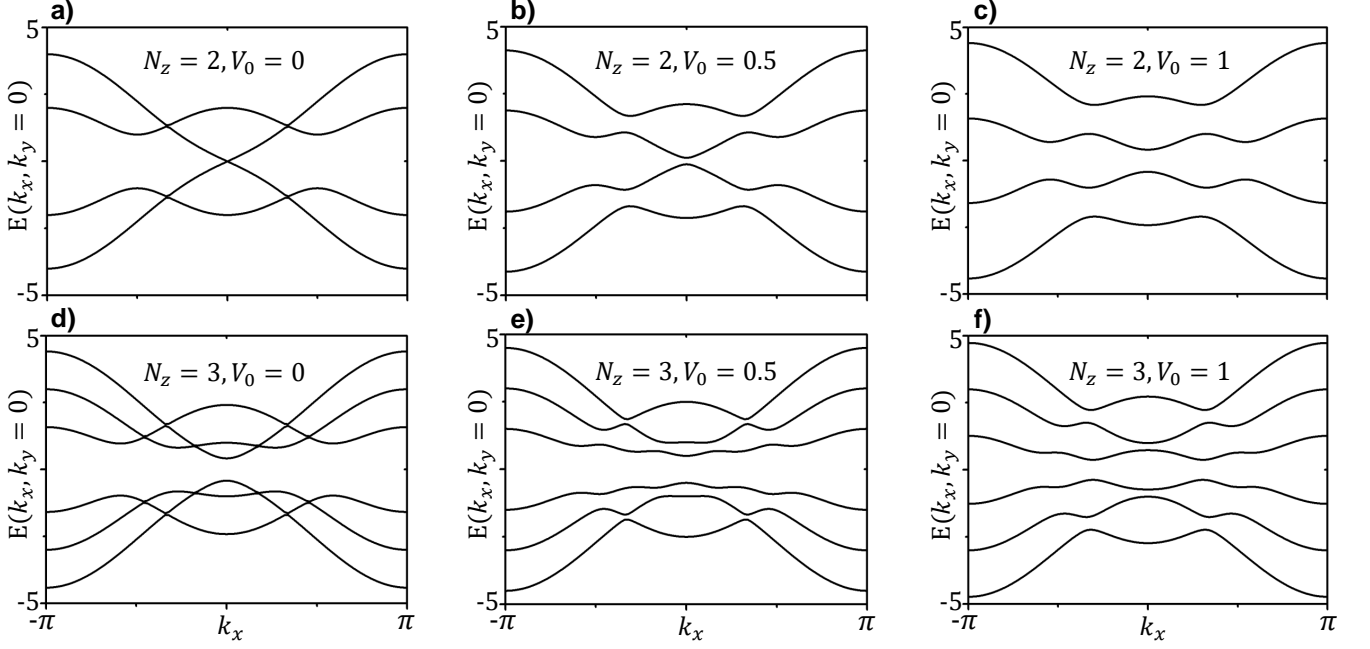


FIG. B1. The evolution of normal-state energy spectra with respect to gate potential for bilayer and trilayer thin films. Chosen parameters are $m = 3$, $t = t_z = 2$, $\lambda = 1$, and $\eta = 0$. The gate voltage cannot lift the spin degeneracy when the η terms are absent.

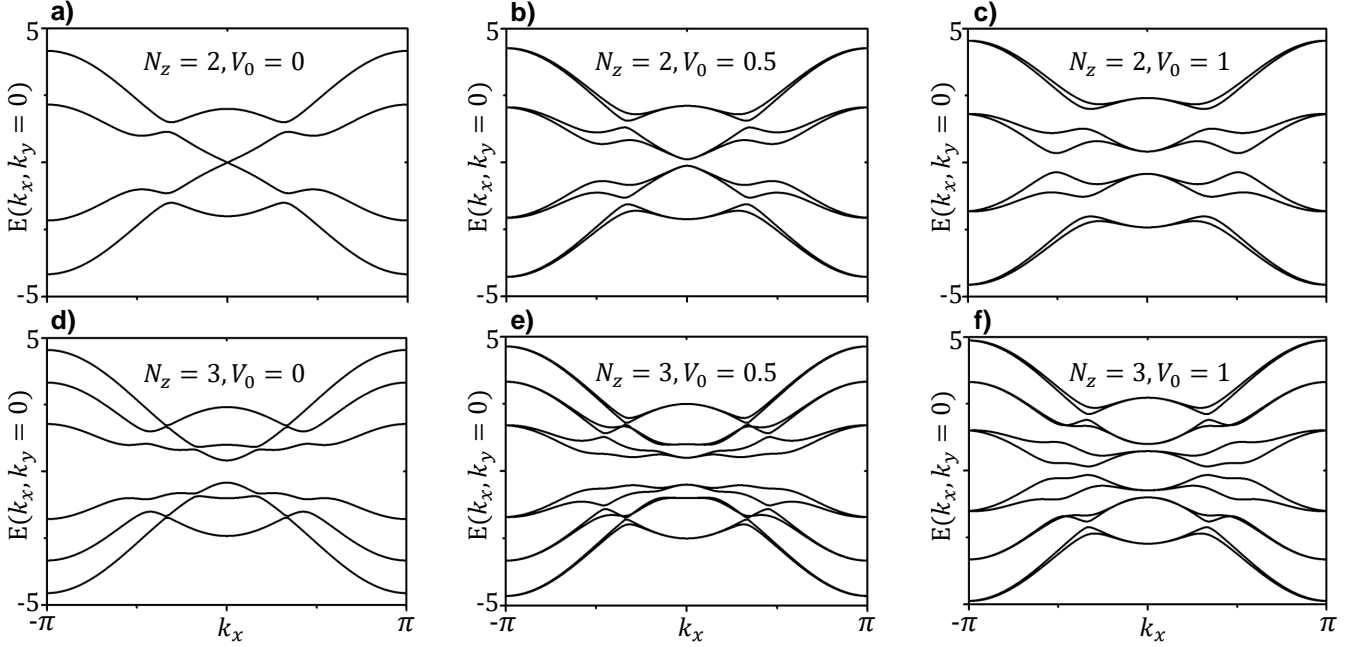


FIG. B2. The evolution of normal-state energy spectra with respect to gate potential for bilayer and trilayer thin films. Chosen parameters are $m = 3$, $t = t_z = 2$, $\lambda = 1$, and $\eta = 1$. The gate voltage lifts the spin degeneracy when the η terms are finite.

We first investigate the energy spectrum of thin-film Dirac semimetals when $\eta = 0$ and superconductivity is absent. To be specific, here we focus on thin films with number of layers $N_z = 2$ and $N_z = 3$. We find that, for both the bilayer and trilayer, while the gate voltage

can strongly modify the dispersions of the energy bands, it cannot lift the spin degeneracy, as shown in Fig. B1. Since the double degeneracy of the energy bands cannot be lifted by the gate voltage, this suggests that when the η terms are absent, the naive approach of using gate volt-

age to drive the superconducting Dirac semimetal with even-parity pairing into a first-order time-reversal invariant topological superconductor does not work.

For comparison, we change η from 0 to 1 and keep other parameters fixed, with the corresponding energy bands shown in Fig. B2. One can see that, for both the bilayer and the trilayer thin films, the double degeneracy of energy bands is lifted by a finite gate voltage, which makes the realization of first-order time-reversal invariant topological superconductivity possible.

To understand the origin of the qualitative difference between the two situations with and without the η terms, here we take the bilayer case for illustration. When $N_z = 2$, in the basis $(c_{a,\uparrow,k_x,k_y,z=1}^\dagger, c_{b,\uparrow,k_x,k_y,z=1}^\dagger, c_{a,\downarrow,k_x,k_y,z=1}^\dagger, c_{b,\downarrow,k_x,k_y,z=1}^\dagger, c_{a,\uparrow,k_x,k_y,z=2}^\dagger, c_{b,\uparrow,k_x,k_y,z=2}^\dagger, c_{a,\downarrow,k_x,k_y,z=2}^\dagger, c_{b,\downarrow,k_x,k_y,z=2}^\dagger)$, the normal-state Hamiltonian can be written as

$$H(\mathbf{k}) = (m - t \cos k_x - t \cos k_y) \sigma_z - \frac{t_z}{2} \rho_x \sigma_z + \lambda (\sin k_x s_z \sigma_x - \sin k_y s_y) + \eta \sin k_x \sin k_y \rho_y s_y \sigma_x + \frac{\eta}{2} (\cos k_x - \cos k_y) \rho_y s_x \sigma_x + V_0 \rho_z, \quad (\text{B1})$$

where the Pauli matrices σ_i , s_i , and ρ_i act on orbital, spin, and layer degrees of freedom, respectively. When $\eta = 0$, although the physical inversion symmetry (the inversion symmetry operator becomes $\tilde{I} = \rho_x \sigma_z$ as it should exchange the two layers) is broken, one finds that the Hamiltonian still commutes with the antiunitary operator $is_y \mathcal{K} \sigma_z$ which is a combination of time-reversal and inversion symmetry in orbital space. The combined symmetry obeys $(is_y \mathcal{K} \sigma_z)^2 = -1$, and the energy bands thus still obey Kramers' degeneracy at each \mathbf{k} . However, once $\eta \neq 0$, the two η terms are odd under that combined symmetry, and lead to a splitting of Kramers' degeneracy.

* yanzhb5@mail.sysu.edu.cn

- ¹ N. Read and Dmitry Green, "Paired states of fermions in two dimensions with breaking of parity and time-reversal symmetries and the fractional quantum Hall effect," *Phys. Rev. B* **61**, 10267–10297 (2000).
- ² Alexei Kitaev, "Unpaired Majorana fermions in quantum wires," *Physics-Uspekhi* **44**, 131 (2001).
- ³ Jason Alicea, "New directions in the pursuit of Majorana fermions in solid state systems," *Reports on Progress in Physics* **75**, 076501 (2012).
- ⁴ Martin Leijnse and Karsten Flensberg, "Introduction to topological superconductivity and Majorana fermions," *Semiconductor Science and Technology* **27**, 124003 (2012).
- ⁵ C. W. J. Beenakker, "Search for Majorana Fermions in Superconductors," *Annual Review of Condensed Matter Physics* **4**, 113–136 (2013).
- ⁶ Tudor D Stanescu and Sumanta Tewari, "Majorana fermions in semiconductor nanowires: fundamentals, modeling, and experiment," *Journal of Physics: Condensed Matter* **25**, 233201 (2013).
- ⁷ Steven R. Elliott and Marcel Franz, "Colloquium : Majorana fermions in nuclear, particle, and solid-state physics," *Rev. Mod. Phys.* **87**, 137–163 (2015).
- ⁸ Masatoshi Sato and Satoshi Fujimoto, "Majorana fermions and topology in superconductors," *Journal of the Physical Society of Japan* **85**, 072001 (2016).
- ⁹ Ramón Aguado, "Majorana quasiparticles in condensed matter," *La Rivista del Nuovo Cimento* **40**, 523–593 (2017).
- ¹⁰ Arbel Haim and Yuval Oreg, "Time-reversal-invariant topological superconductivity in one and two dimensions," *Physics Reports* **825**, 1–48 (2019).
- ¹¹ Berthold Jäck, Yonglong Xie, and Ali Yazdani, "Detecting and distinguishing Majorana zero modes with the scanning tunneling microscope," *arXiv preprint arXiv:2103.13210* (2021).
- ¹² D. A. Ivanov, "Non-Abelian statistics of half-quantum vortices in p -wave superconductors," *Phys. Rev. Lett.* **86**, 268–271 (2001).
- ¹³ Jason Alicea, Yuval Oreg, Gil Refael, Felix von Oppen, and Matthew P. A. Fisher, "Non-Abelian statistics and topological quantum information processing in 1D wire networks," *Nature Physics* **7**, 412–417 (2011).
- ¹⁴ Chetan Nayak, Steven H. Simon, Ady Stern, Michael Freedman, and Sankar Das Sarma, "Non-Abelian anyons and topological quantum computation," *Rev. Mod. Phys.* **80**, 1083–1159 (2008).
- ¹⁵ Sankar Das Sarma, Michael Freedman, and Chetan Nayak, "Majorana zero modes and topological quantum computation," *npj Quantum Information* **1**, 15001 (2015).
- ¹⁶ Wladimir A. Benalcazar, B. Andrei Bernevig, and Taylor L. Hughes, "Quantized electric multipole insulators," *Science* **357**, 61–66 (2017).
- ¹⁷ Frank Schindler, Ashley M. Cook, Maia G. Vergniory, Zhi-jun Wang, Stuart S. P. Parkin, B. Andrei Bernevig, and Titus Neupert, "Higher-order topological insulators," *Science Advances* **4** (2018), 10.1126/sciadv.aat0346.
- ¹⁸ Wladimir A. Benalcazar, B. Andrei Bernevig, and Taylor L. Hughes, "Electric multipole moments, topological multipole moment pumping, and chiral hinge states in crystalline insulators," *Phys. Rev. B* **96**, 245115 (2017).
- ¹⁹ Zhida Song, Zhong Fang, and Chen Fang, " $(d-2)$ -dimensional edge states of rotation symmetry protected topological states," *Phys. Rev. Lett.* **119**, 246402 (2017).
- ²⁰ J. Langbehn, Yang Peng, L. Trifunovic, Felix von Oppen, and Piet W. Brouwer, "Reflection-symmetric second-

- order topological insulators and superconductors,” *Phys. Rev. Lett.* **119**, 246401 (2017).
- ²¹ Eslam Khalaf, “Higher-order topological insulators and superconductors protected by inversion symmetry,” *Phys. Rev. B* **97**, 205136 (2018).
 - ²² Max Geier, Luka Trifunovic, Max Hoskam, and Piet W. Brouwer, “Second-order topological insulators and superconductors with an order-two crystalline symmetry,” *Phys. Rev. B* **97**, 205135 (2018).
 - ²³ Xiaoyu Zhu, “Tunable Majorana corner states in a two-dimensional second-order topological superconductor induced by magnetic fields,” *Phys. Rev. B* **97**, 205134 (2018).
 - ²⁴ Zhongbo Yan, Fei Song, and Zhong Wang, “Majorana corner modes in a high-temperature platform,” *Phys. Rev. Lett.* **121**, 096803 (2018).
 - ²⁵ Qiyue Wang, Cheng-Cheng Liu, Yuan-Ming Lu, and Fan Zhang, “High-temperature Majorana corner states,” *Phys. Rev. Lett.* **121**, 186801 (2018).
 - ²⁶ Yuxuan Wang, Mao Lin, and Taylor L. Hughes, “Weak-pairing higher order topological superconductors,” *Phys. Rev. B* **98**, 165144 (2018).
 - ²⁷ Zhongbo Yan, “Higher-order topological odd-parity superconductors,” *Phys. Rev. Lett.* **123**, 177001 (2019).
 - ²⁸ Hassan Shapourian, Yuxuan Wang, and Shinsei Ryu, “Topological crystalline superconductivity and second-order topological superconductivity in nodal-loop materials,” *Phys. Rev. B* **97**, 094508 (2018).
 - ²⁹ Chen-Hsuan Hsu, Peter Stano, Jelena Klinovaja, and Daniel Loss, “Majorana Kramers pairs in higher-order topological insulators,” *Phys. Rev. Lett.* **121**, 196801 (2018).
 - ³⁰ Tao Liu, James Jun He, and Franco Nori, “Majorana corner states in a two-dimensional magnetic topological insulator on a high-temperature superconductor,” *Phys. Rev. B* **98**, 245413 (2018).
 - ³¹ Zhigang Wu, Zhongbo Yan, and Wen Huang, “Higher-order topological superconductivity: Possible realization in Fermi gases and Sr_2RuO_4 ,” *Phys. Rev. B* **99**, 020508 (2019).
 - ³² Rui-Xing Zhang, William S. Cole, and S. Das Sarma, “Helical hinge Majorana modes in iron-based superconductors,” *Phys. Rev. Lett.* **122**, 187001 (2019).
 - ³³ Rui-Xing Zhang, William S. Cole, Xianxin Wu, and S. Das Sarma, “Higher-order topology and nodal topological superconductivity in $\text{Fe}(\text{Se},\text{Te})$ heterostructures,” *Phys. Rev. Lett.* **123**, 167001 (2019).
 - ³⁴ Yanick Volpez, Daniel Loss, and Jelena Klinovaja, “Second-order topological superconductivity in π -junction Rashba layers,” *Phys. Rev. Lett.* **122**, 126402 (2019).
 - ³⁵ Xiaoyu Zhu, “Second-order topological superconductors with mixed pairing,” *Phys. Rev. Lett.* **122**, 236401 (2019).
 - ³⁶ Yang Peng and Yong Xu, “Proximity-induced Majorana hinge modes in antiferromagnetic topological insulators,” *Phys. Rev. B* **99**, 195431 (2019).
 - ³⁷ Sayed Ali Akbar Ghorashi, Xiang Hu, Taylor L. Hughes, and Enrico Rossi, “Second-order Dirac superconductors and magnetic field induced Majorana hinge modes,” *Phys. Rev. B* **100**, 020509 (2019).
 - ³⁸ Zhongbo Yan, “Majorana corner and hinge modes in second-order topological insulator/superconductor heterostructures,” *Phys. Rev. B* **100**, 205406 (2019).
 - ³⁹ Nick Bultinck, B. Andrei Bernevig, and Michael P. Zaletel, “Three-dimensional superconductors with hybrid higher-order topology,” *Phys. Rev. B* **99**, 125149 (2019).
 - ⁴⁰ S. Franca, D. V. Efremov, and I. C. Fulga, “Phase-tunable second-order topological superconductor,” *Phys. Rev. B* **100**, 075415 (2019).
 - ⁴¹ Xiao-Hong Pan, Kai-Jie Yang, Li Chen, Gang Xu, Chao-Xing Liu, and Xin Liu, “Lattice-symmetry-assisted second-order topological superconductors and Majorana patterns,” *Phys. Rev. Lett.* **123**, 156801 (2019).
 - ⁴² Majid Kheirkhah, Yuki Nagai, Chun Chen, and Frank Marsiglio, “Majorana corner flat bands in two-dimensional second-order topological superconductors,” *Phys. Rev. B* **101**, 104502 (2020).
 - ⁴³ Majid Kheirkhah, Zhongbo Yan, Yuki Nagai, and Frank Marsiglio, “First- and second-order topological superconductivity and temperature-driven topological phase transitions in the extended Hubbard model with spin-orbit coupling,” *Phys. Rev. Lett.* **125**, 017001 (2020).
 - ⁴⁴ Ya-Jie Wu, Junpeng Hou, Yun-Mei Li, Xi-Wang Luo, Xiaoyan Shi, and Chuanwei Zhang, “In-plane Zeeman-field-induced Majorana corner and hinge modes in an s -wave superconductor heterostructure,” *Phys. Rev. Lett.* **124**, 227001 (2020).
 - ⁴⁵ Yi-Ting Hsu, William S. Cole, Rui-Xing Zhang, and Jay D. Sau, “Inversion-protected higher-order topological superconductivity in monolayer WTe_2 ,” *Phys. Rev. Lett.* **125**, 097001 (2020).
 - ⁴⁶ Xianxin Wu, Wladimir A. Benalcazar, Yinxian Li, Ronny Thomale, Chao-Xing Liu, and Jiangping Hu, “Boundary-obstructed topological high- T_c superconductivity in iron pnictides,” *Phys. Rev. X* **10**, 041014 (2020).
 - ⁴⁷ Katharina Laubscher, Daniel Chughtai, Daniel Loss, and Jelena Klinovaja, “Kramers pairs of Majorana corner states in a topological insulator bilayer,” *Phys. Rev. B* **102**, 195401 (2020).
 - ⁴⁸ Apoorv Tiwari, Ammar Jahin, and Yuxuan Wang, “Chiral Dirac superconductors: Second-order and boundary-obstructed topology,” *Phys. Rev. Research* **2**, 043300 (2020).
 - ⁴⁹ Junyeong Ahn and Bohm-Jung Yang, “Higher-order topological superconductivity of spin-polarized fermions,” *Phys. Rev. Research* **2**, 012060 (2020).
 - ⁵⁰ Bitan Roy, “Higher-order topological superconductors in \mathcal{P} -, T -odd quadrupolar Dirac materials,” *Phys. Rev. B* **101**, 220506 (2020).
 - ⁵¹ Bo-Xuan Li and Zhongbo Yan, “Boundary topological superconductors,” *Phys. Rev. B* **103**, 064512 (2021).
 - ⁵² Jingjing Niu, Tongxing Yan, Yuxuan Zhou, Ziyu Tao, Xiaole Li, Weiyang Liu, Libo Zhang, Hao Jia, Song Liu, Zhongbo Yan, *et al.*, “Simulation of higher-order topological phases and related topological phase transitions in a superconducting qubit,” *Science Bulletin* **66**, 1168–1175 (2021).
 - ⁵³ Xianxin Wu, Xin Liu, Ronny Thomale, and Chao-Xing Liu, “High- T_c superconductor $\text{Fe}(\text{Se},\text{Te})$ Monolayer: an intrinsic, scalable and electrically-tunable Majorana platform,” *National Science Review*, 2095–5138 (2021).
 - ⁵⁴ Bo Fu, Zi-Ang Hu, Chang-An Li, Jian Li, and Shun-Qing Shen, “Chiral Majorana hinge modes in superconducting Dirac materials,” *Phys. Rev. B* **103**, L180504 (2021).
 - ⁵⁵ Xun-Jiang Luo, Xiao-Hong Pan, and Xin Liu, “Higher-order topological superconductors based on weak topological insulators,” *arXiv preprint arXiv:2103.01825* (2021).

- ⁵⁶ Ammar Jahin, Apoorv Tiwari, and Yuxuan Wang, “Higher-order topological superconductors from Weyl semimetals,” [arXiv preprint arXiv:2103.05010](#) (2021).
- ⁵⁷ Shengshan Qin, Chen Fang, Fu-Chun Zhang, and Jiangping Hu, “Topological superconductivity in an s -wave superconductor and its implication to iron-based superconductors,” [arXiv preprint arXiv:2106.04200](#) (2021).
- ⁵⁸ Yi Tan, Zhi-Hao Huang, and Xiong-Jun Liu, “Edge geometric phase mechanism for second-order topological insulator and superconductor,” [arXiv preprint arXiv:2106.12507](#) (2021).
- ⁵⁹ Yizhi You, Daniel Litinski, and Felix von Oppen, “Higher-order topological superconductors as generators of quantum codes,” *Phys. Rev. B* **100**, 054513 (2019).
- ⁶⁰ Song-Bo Zhang, Alessio Calzona, and Björn Trauzettel, “All-electrically tunable networks of Majorana bound states,” *Phys. Rev. B* **102**, 100503 (2020).
- ⁶¹ Song-Bo Zhang, W. B. Rui, Alessio Calzona, Sang-Jun Choi, Andreas P. Schnyder, and Björn Trauzettel, “Topological and holonomic quantum computation based on second-order topological superconductors,” *Phys. Rev. Research* **2**, 043025 (2020).
- ⁶² Tudor E. Pahomi, Manfred Sigrist, and Alexey A. Soluyanov, “Braiding Majorana corner modes in a second-order topological superconductor,” *Phys. Rev. Research* **2**, 032068 (2020).
- ⁶³ Raditya Weda Bomantara and Jiangbin Gong, “Measurement-only quantum computation with Floquet Majorana corner modes,” *Phys. Rev. B* **101**, 085401 (2020).
- ⁶⁴ Matthew F Lapa, Meng Cheng, and Yuxuan Wang, “Symmetry-protected gates of Majorana qubits in a high- T_c superconductor platform,” [arXiv preprint arXiv:2103.03893](#) (2021).
- ⁶⁵ S. Ikegaya, W. B. Rui, D. Manske, and Andreas P. Schnyder, “Tunable Majorana corner modes in noncentrosymmetric superconductors: Tunneling spectroscopy and edge imperfections,” *Phys. Rev. Research* **3**, 023007 (2021).
- ⁶⁶ Bitan Roy and Vladimir Juricic, “Mixed parity octupolar pairing and corner Majorana modes in three dimensions,” [arXiv preprint arXiv:2106.01361](#) (2021).
- ⁶⁷ Liang Fu and C. L. Kane, “Superconducting proximity effect and Majorana fermions at the surface of a topological insulator,” *Phys. Rev. Lett.* **100**, 096407 (2008).
- ⁶⁸ Roman M. Lutchyn, Tudor D. Stanescu, and S. Das Sarma, “Search for Majorana fermions in multi-band semiconducting nanowires,” *Phys. Rev. Lett.* **106**, 127001 (2011).
- ⁶⁹ Yuval Oreg, Gil Refael, and Felix von Oppen, “Helical liquids and Majorana bound states in quantum wires,” *Phys. Rev. Lett.* **105**, 177002 (2010).
- ⁷⁰ Jay D. Sau, Roman M. Lutchyn, Sumanta Tewari, and S. Das Sarma, “Generic new platform for topological quantum computation using semiconductor heterostructures,” *Phys. Rev. Lett.* **104**, 040502 (2010).
- ⁷¹ Jason Alicea, “Majorana fermions in a tunable semiconductor device,” *Phys. Rev. B* **81**, 125318 (2010).
- ⁷² V. Mourik, K. Zuo, S. M. Frolov, S. R. Plissard, E. P. A. M. Bakkers, and L. P. Kouwenhoven, “Signatures of Majorana fermions in hybrid superconductor-semiconductor nanowire devices,” *Science* **336**, 1003–1007 (2012).
- ⁷³ Leonid P Rokhinson, Xinyu Liu, and Jacek K Furdyna, “The fractional ac Josephson effect in a semiconductor-superconductor nanowire as a signature of Majorana particles,” *Nature Physics* **8**, 795–799 (2012).
- ⁷⁴ Anindya Das, Yuval Ronen, Yonatan Most, Yuval Oreg, Moty Heiblum, and Hadas Shtrikman, “Zero-bias peaks and splitting in an Al-InAs nanowire topological superconductor as a signature of Majorana fermions,” *Nature Physics* **8**, 887–895 (2012).
- ⁷⁵ MT Deng, CL Yu, GY Huang, Marcus Larsson, Philippe Caroff, and HQ Xu, “Anomalous zero-bias conductance peak in a Nb-InSb nanowire-Nb hybrid device,” *Nano letters* **12**, 6414–6419 (2012).
- ⁷⁶ A. D. K. Finck, D. J. Van Harlingen, P. K. Mohseni, K. Jung, and X. Li, “Anomalous modulation of a zero-bias peak in a hybrid nanowire-superconductor device,” *Phys. Rev. Lett.* **110**, 126406 (2013).
- ⁷⁷ Stevan Nadj-Perge, Ilya K Drozdov, Jian Li, Hua Chen, Sangjun Jeon, Jungpil Seo, Allan H MacDonald, B Andrei Bernevig, and Ali Yazdani, “Observation of Majorana fermions in ferromagnetic atomic chains on a superconductor,” *Science* **346**, 602–607 (2014).
- ⁷⁸ Hao-Hua Sun, Kai-Wen Zhang, Lun-Hui Hu, Chuang Li, Guan-Yong Wang, Hai-Yang Ma, Zhu-An Xu, Chun-Lei Gao, Dan-Dan Guan, Yao-Yi Li, Canhua Liu, Dong Qian, Yi Zhou, Liang Fu, Shao-Chun Li, Fu-Chun Zhang, and Jin-Feng Jia, “Majorana zero mode detected with spin selective Andreev reflection in the vortex of a topological superconductor,” *Phys. Rev. Lett.* **116**, 257003 (2016).
- ⁷⁹ MT Deng, S Vaitiekėnas, EB Hansen, J Danon, M Leijnse, K Flensberg, J Nygård, P Krogstrup, and CM Marcus, “Majorana bound state in a coupled quantum-dot hybrid-nanowire system,” *Science* **354**, 1557–1562 (2016).
- ⁸⁰ Antonio Fornieri, Alexander M. Whicar, F. Setiawan, Elías Portolés, Asbjørn C. C. Drachmann, Anna Keselman, Sergei Gronin, Candice Thomas, Tian Wang, Ray Kallaher, Geoffrey C. Gardner, Erez Berg, Michael J. Manfra, Ady Stern, Charles M. Marcus, and Fabrizio Nichele, “Evidence of topological superconductivity in planar Josephson junctions,” *Nature* **569**, 89–92 (2019).
- ⁸¹ Hechen Ren, Falko Pientka, Sean Hart, Andrew T. Pierce, Michael Kosowsky, Lukas Lunczer, Raimund Schlereth, Benedikt Scharf, Ewelina M. Hankiewicz, Laurens W. Molenkamp, Bertrand I. Halperin, and Amir Yacoby, “Topological superconductivity in a phase-controlled Josephson junction,” *Nature* **569**, 93–98 (2019).
- ⁸² Hao Zhang, Dong E. Liu, Michael Wimmer, and Leo P. Kouwenhoven, “Next steps of quantum transport in Majorana nanowire devices,” *Nature Communications* **10**, 5128 (2019).
- ⁸³ S. M. Frolov, M. J. Manfra, and J. D. Sau, “Topological superconductivity in hybrid devices,” *Nature Physics* **16**, 718–724 (2020).
- ⁸⁴ P. Yu, J. Chen, M. Gomanko, G. Badawy, E. P. A. M. Bakkers, K. Zuo, V. Mourik, and S. M. Frolov, “Non-Majorana states yield nearly quantized conductance in proximatized nanowires,” *Nature Physics* **17**, 482–488 (2021).
- ⁸⁵ Peng Zhang, Koichiro Yaji, Takahiro Hashimoto, Yuichi Ota, Takeshi Kondo, Kozo Okazaki, Zhijun Wang, Jinsheng Wen, GD Gu, Hong Ding, *et al.*, “Observation of topological superconductivity on the surface of an iron-based superconductor,” *Science* **360**, 182–186 (2018).
- ⁸⁶ Peng Zhang, Zhijun Wang, Xianxin Wu, Koichiro Yaji, Yukiaki Ishida, Yoshimitsu Kohama, Guangyang Dai, Yue Sun, Cedric Bareille, Kenta Kuroda, *et al.*, “Multiple

- topological states in iron-based superconductors,” *Nature Physics* **15**, 41 (2019).
- ⁸⁷ Dongfei Wang, Lingyuan Kong, Peng Fan, Hui Chen, Shiyu Zhu, Wenyao Liu, Lu Cao, Yujie Sun, Shixuan Du, John Schneeloch, *et al.*, “Evidence for Majorana bound states in an iron-based superconductor,” *Science* **362**, 333–335 (2018).
- ⁸⁸ Qin Liu, Chen Chen, Tong Zhang, Rui Peng, Ya-Jun Yan, Chen-Hao-Ping Wen, Xia Lou, Yu-Long Huang, Jin-Peng Tian, Xiao-Li Dong, Guang-Wei Wang, Wei-Cheng Bao, Qiang-Hua Wang, Zhi-Ping Yin, Zhong-Xian Zhao, and Dong-Lai Feng, “Robust and clean Majorana zero mode in the vortex core of high-temperature superconductor ($\text{Li}_{0.84}\text{Fe}_{0.16}\text{OHFeSe}$),” *Phys. Rev. X* **8**, 041056 (2018).
- ⁸⁹ T Machida, Y Sun, S Pyon, S Takeda, Y Kohsaka, T Hanaguri, T Sasagawa, and T Tamegai, “Zero-energy vortex bound state in the superconducting topological surface state of $\text{Fe}(\text{Se}, \text{Te})$,” *Nature materials* **18**, 811–815 (2019).
- ⁹⁰ Lingyuan Kong, Shiyu Zhu, Michał Papaj, Hui Chen, Lu Cao, Hiroki Isobe, Yuqing Xing, Wenyao Liu, Dongfei Wang, Peng Fan, *et al.*, “Half-integer level shift of vortex bound states in an iron-based superconductor,” *Nature Physics* **15**, 1181–1187 (2019).
- ⁹¹ Shiyu Zhu, Lingyuan Kong, Lu Cao, Hui Chen, Michał Papaj, Shixuan Du, Yuqing Xing, Wenyao Liu, Dongfei Wang, Chengmin Shen, Fazhi Yang, John Schneeloch, Ruidan Zhong, Genda Gu, Liang Fu, Yu-Yang Zhang, Hong Ding, and Hong-Jun Gao, “Nearly quantized conductance plateau of vortex zero mode in an iron-based superconductor,” *Science* **367**, 189–192 (2020).
- ⁹² Kun Jiang, Xi Dai, and Ziqiang Wang, “Quantum anomalous vortex and Majorana zero mode in iron-based superconductor $\text{Fe}(\text{Te}, \text{Se})$,” *Phys. Rev. X* **9**, 011033 (2019).
- ⁹³ Shengshan Qin, Lunhui Hu, Xianxin Wu, Xia Dai, Chen Fang, Fu-Chun Zhang, and Jiangping Hu, “Topological vortex phase transitions in iron-based superconductors,” *Science Bulletin* **64**, 1207 – 1214 (2019).
- ⁹⁴ Ching-Kai Chiu, T Machida, Yingyi Huang, T Hanaguri, and Fu-Chun Zhang, “Scalable Majorana vortex modes in iron-based superconductors,” *Science Advances* **6**, eaay0443 (2020).
- ⁹⁵ Areg Ghazaryan, P. L. S. Lopes, Pavan Hosur, Matthew J. Gilbert, and Pouyan Ghaemi, “Effect of zeeman coupling on the Majorana vortex modes in iron-based topological superconductors,” *Phys. Rev. B* **101**, 020504 (2020).
- ⁹⁶ Xianxin Wu, Suk Bum Chung, Chaoxing Liu, and Eun-Ah Kim, “Topological orders competing for the Dirac surface state in FeSeTe surfaces,” *Phys. Rev. Research* **3**, 013066 (2021).
- ⁹⁷ Majid Kheirkhah, Zhongbo Yan, and Frank Marsiglio, “Vortex-line topology in iron-based superconductors with and without second-order topology,” *Phys. Rev. B* **103**, L140502 (2021).
- ⁹⁸ Shengshan Qin, Lunhui Hu, Congcong Le, Jinfeng Zeng, Fu-chun Zhang, Chen Fang, and Jiangping Hu, “Quasi-1D topological nodal vortex line phase in doped superconducting 3D Dirac semimetals,” *Phys. Rev. Lett.* **123**, 027003 (2019).
- ⁹⁹ Elio J. König and Piers Coleman, “Crystalline-Symmetry-Protected Helical Majorana Modes in the Iron Pnictides,” *Phys. Rev. Lett.* **122**, 207001 (2019).
- ¹⁰⁰ Zhongbo Yan, Zhigang Wu, and Wen Huang, “Vortex end Majorana zero modes in superconducting Dirac and Weyl semimetals,” *Phys. Rev. Lett.* **124**, 257001 (2020).
- ¹⁰¹ Takuto Kawakami and Masatoshi Sato, “Topological crystalline superconductivity in Dirac semimetal phase of iron-based superconductors,” *Phys. Rev. B* **100**, 094520 (2019).
- ¹⁰² Bohm-Jung Yang and Naoto Nagaosa, “Classification of stable three-dimensional Dirac semimetals with nontrivial topology,” *Nature Communications* **5**, 4898 (2014).
- ¹⁰³ Shingo Kobayashi and Masatoshi Sato, “Topological superconductivity in Dirac semimetals,” *Phys. Rev. Lett.* **115**, 187001 (2015).
- ¹⁰⁴ Mehdi Kargarian, Mohit Randeria, and Yuan-Ming Lu, “Are the surface Fermi arcs in Dirac semimetals topologically protected?” *Proceedings of the National Academy of Sciences* **113**, 8648–8652 (2016).
- ¹⁰⁵ Benjamin J. Wieder, Zhijun Wang, Jennifer Cano, Xi Dai, Leslie M. Schoop, Barry Bradlyn, and B. Andrei Bernevig, “Strong and fragile topological Dirac semimetals with higher-order Fermi arcs,” *Nature Communications* **11**, 627 (2020).
- ¹⁰⁶ Congcong Le, Xianxin Wu, Shengshan Qin, Yinxian Li, Ronny Thomale, Fu-Chun Zhang, and Jiangping Hu, “Dirac semimetal in $\beta\text{-CuI}$ without surface fermi arcs,” *Proceedings of the National Academy of Sciences* **115**, 8311–8315 (2018).
- ¹⁰⁷ Andreas P. Schnyder, Shinsei Ryu, Akira Furusaki, and Andreas W. W. Ludwig, “Classification of topological insulators and superconductors in three spatial dimensions,” *Phys. Rev. B* **78**, 195125 (2008).
- ¹⁰⁸ Alexei Kitaev, “Periodic table for topological insulators and superconductors,” in *AIP Conference Proceedings*, Vol. 1134 (AIP, 2009) pp. 22–30.
- ¹⁰⁹ Rahul Roy, “Topological superfluids with time reversal symmetry,” *arXiv:0803.2868* (2008).
- ¹¹⁰ Xiao-Liang Qi, Taylor L. Hughes, S. Raghu, and Shou-Cheng Zhang, “Time-reversal-invariant topological superconductors and superfluids in two and three dimensions,” *Phys. Rev. Lett.* **102**, 187001 (2009).
- ¹¹¹ G. E. Volovik, “Fermion zero modes at the boundary of superfluid $^3\text{He-B}$,” *JETP Lett.* **90**, 398–401 (2009).
- ¹¹² Xiao-Liang Qi, Taylor L. Hughes, and Shou-Cheng Zhang, “Topological invariants for the fermi surface of a time-reversal-invariant superconductor,” *Phys. Rev. B* **81**, 134508 (2010).
- ¹¹³ FDM Haldane, “Attachment of Surface “Fermi Arcs” to the Bulk Fermi Surface: “Fermi-Level Plumbing” in Topological Metals,” *arXiv preprint arXiv:1401.0529* (2014).
- ¹¹⁴ Shinsei Ryu, Andreas Schnyder, Akira Furusaki, and Andreas Ludwig, “Topological insulators and superconductors: ten-fold way and dimensional hierarchy,” *New J. Phys.* **12**, 065010 (2010).
- ¹¹⁵ Shun-Qing Shen, *Topological Insulators: Dirac Equation in Condensed Matters*, Vol. 174 (Springer Science & Business Media, 2013).
- ¹¹⁶ Rui-Xing Zhang and S. Das Sarma, “Intrinsic time-reversal-invariant topological superconductivity in thin films of iron-based superconductors,” *Phys. Rev. Lett.* **126**, 137001 (2021).
- ¹¹⁷ Sho Nakosai, Yukio Tanaka, and Naoto Nagaosa, “Topological superconductivity in bilayer Rashba system,” *Phys. Rev. Lett.* **108**, 147003 (2012).
- ¹¹⁸ Fan Zhang, C. L. Kane, and E. J. Mele, “Time-reversal-invariant topological superconductivity and Majorana Kramers pairs,” *Phys. Rev. Lett.* **111**, 056402 (2013).

- ¹¹⁹ Jing Wang, Yong Xu, and Shou-Cheng Zhang, “Two-dimensional time-reversal-invariant topological superconductivity in a doped quantum spin-Hall insulator,” *Phys. Rev. B* **90**, 054503 (2014).
- ¹²⁰ Fariborz Parhizgar and Annica M. Black-Schaffer, “Highly tunable time-reversal-invariant topological superconductivity in topological insulator thin films,” *Scientific Reports* **7**, 9817 (2017).
- ¹²¹ Oscar E. Casas, Liliana Arrachea, William J. Herrera, and Alfredo Levy Yeyati, “Proximity induced time-reversal topological superconductivity in Bi_2Se_3 films without phase tuning,” *Phys. Rev. B* **99**, 161301 (2019).
- ¹²² Shawulienu Kezilebieke, Md Nurul Huda, Viliam Vaňo, Markus Aapro, Somesh C. Ganguli, Orlando J. Silveira, Szczepan Głodzik, Adam S. Foster, Teemu Ojanen, and Peter Liljeroth, “Topological superconductivity in a van der Waals heterostructure,” *Nature* **588**, 424–428 (2020).
- ¹²³ Mason J. Gray, Josef Freudenstein, Shu Yang F. Zhao, Ryan O’Connor, Samuel Jenkins, Narendra Kumar, Marcel Hoek, Abigail Kopec, Soonsang Huh, Takashi Taniguchi, Kenji Watanabe, Ruidan Zhong, Changyoung Kim, G. D. Gu, and K. S. Burch, “Evidence for helical hinge zero modes in an Fe-based superconductor,” *Nano Letters* **19**, 4890–4896 (2019).